Differential modifications of the C-terminal tails of α-tubulin isoforms and their *in vivo* importance for kinesin function in *Drosophila*

Mengjing Bao, Ruth Dörig, Dirk Beuchle, Paula Maria Vazquez-Pianzola and Beat Suter

Institute of Cell Biology, University of Bern, Switzerland

Summary

Drosophila TTLL5 is required for:

1. α-tubulin glutamylation in *vivo,* specifically on the C-terminal domain of TBA1 and 3; the female germline isoform TBA4 is not glutamylated.

2. Kinesin-based localization of Staufen/*osk* mRNA and ooplasmic streaming during oogenesis.

3. Kinesin-based transport of mitochondria in neurons.

Abstract

Microtubules (MTs) are built from α-/β-tubulin dimers and used as tracks by kinesin and dynein motors to transport a variety of cargos, such as mRNAs, proteins, and organelles, within the cell. Tubulins are subjected to several post-translational modifications (PTMs). Glutamylation is one of them and it is responsible for adding one or more glutamic acids as branched peptide chains to the C-terminal tails of both α- and β-tubulin. However, very little is known about the specific modifications found on the different tubulin isoforms *in vivo* and the role of these PTMs in cargo transport along MTs *in vivo*. In this study, we found that *Drosophila TTLL5* is required specifically for the glutamylation of the α-tubulin isoforms TBA1 and TBA3 in ovaries, whereas the ovarian isoform TBA4 is not glutamylated. Furthermore, *TTLL5* is essential for the efficient localization of Staufen/*osk* mRNA and to give directionality to the fast ooplasmic streaming, two processes known to depend on kinesin-mediated processes during oogenesis. In the nervous system, the kinesin-dependent neuronal transport of mitochondria also depends on *TTLL5*. Additionally, α-tubulin glutamylation plays a role in controlling the pausing of the transport of individual

mitochondria. Our results demonstrate the *in vivo* role of *TTLL5* in differential glutamylation of α-tubulin isoforms and point to the *in vivo* importance of α-tubulin glutamylation for kinesin-dependent processes.

Introduction

Microtubules (MTs) are key cytoskeletal filaments that are comprised of heterodimers of α- and β-tubulins. Despite the high level of conservation in eukaryotes, MTs are still quite diverse because cells express different isoforms, and these can undergo several different post-translational modifications (PTMs). Based mainly on *in vitro* assays, these isoform variations are thought to optimize the MT interaction with different microtubule-associated proteins (MAPs) and motors.

Drosophila melanogaster possesses four α-tubulin genes. Three of them are expressed during oogenesis and early embryogenesis, suggesting that they contribute to the formation of microtubules during these stages. The three genes are *αTub84B*, *αTub84D,* and *αTub67C* (Kalfayan and Wensink, 1982). *αTub84B* and *αTub84D* encode the TBA1 and TBA3 isoforms of α-tubulin, respectively, which differ in only two amino acids. Their primary sequence in the C-terminal domain is identical and both are expressed in most tissues and throughout development. In contrast, *αTub67C* encodes TBA4 and is expressed exclusively during oogenesis where it is maternally loaded into the egg and embryo. The primary structure of TBA4 is distinctively different from TBA1/3 (Theurkauf et al., 1986). These differences are also apparent in the C-terminal domain and include the last residue, which is phenylalanine (Phe, F) in TBA4 and tyrosine (Tyr, Y) in TBA1/3. *αTub85E,* which encodes TBA2, is mainly expressed in testes (Kalfayan and Wensink, 1982).

MTs are subjected to several PTMs, including the C-terminal tail glutamylation, glycylation, and detyrosination / tyrosination (Arce et al., 1975, Eddé et al., 1990, Redeker et al., 1994, Hallak et al., 1977). Furthermore, acetylation and phosphorylation in the more central parts of the tubulins have also been identified (Arce et al., 1975; Eddé et al., 1990; Hallak et al., 1977; L'Hernault and Rosenbaum, 1985; Magiera and Janke, 2014; Redeker et al., 1994). Glutamylation is a PTM that adds one or more glutamic acids (Glu, E) to the side chains of glutamic acid residues in the C-terminal tails of both α and β tubulin, causing the formation of a branched peptide chain (Eddé et al., 1990; Redeker et al., 1992). Glycylation is another PTM that adds glycines to the γ-carboxyl group of glutamic acid residues in the C-

terminal region (Redeker et al., 1994). At least in vertebrates, tubulin is also subjected to a special cycle of de-tyrosination-tyrosination (Preston et al., 1979). In this case, the C-terminal Tyr or Phe of α-tubulin is cyclically removed, resulting in a C-terminal Glu residue, and a new Tyr can be re-added to the new C-term. The enzymes that catalyze glutamylation, glycylation, and tyrosination belong to the Tubulin-tyrosine-ligase-like (TTLL) family (Janke et al., 2005). In *Drosophila melanogaster*, this family encompasses 11 genes (flybase.org).

CG31108 is considered to be the homolog of the mammalian *TTLL5* gene and was therefore named *DmTTLL5 or TTLL5* (Devambez et al., 2017). It is required for α-tubulin glutamylation in the *Drosophila* nervous system (Devambez et al., 2017). The murine TTLL5 is composed of an N-terminal core tubulin tyrosination ligase-like (TTLL) domain, a cofactor interaction domain (CID), and a C-terminal receptor interaction domain (RID) (Lee et al., 2013). The N-terminal core domain was shown to provide the catalytic activity of TTLL5 and is highly conserved in *Drosophila* TTLL5 (van Dijk et al., 2007) (**Table 1**). According to the FlyBase data, *Drosophila TTLL5* mRNA is expressed at high levels in ovaries (**Table S2**), even higher than in the nervous system where initial studies were performed (Devambez et al., 2017). We thus focused on *TTLL5*'s possible functions during *Drosophila* oogenesis to shed light on possible *in vivo* roles of glutamylated α-tubulins.

MTs have an intrinsic polarity with a plus and a minus end. On these tracks, kinesin motors transport cargo to the plus ends and dynein motors move cargo towards minus ends. Evidence for the importance of PTMs of tubulin subunits has been reported already *in vitro.* Artificial tethering of 10E peptides to the side chains at position E445 of α-tubulin and E435 of β-tubulin by maleimide chemistry increased the processivity (the run length) of kinesin motors on tubulin. For Kinesin-1 this was a 1.5-fold increase (Sirajuddin et al., 2014). In contrast to Kinesin, Dynein/dynactin motors preferred a Tyr at the C-term of α-tubulin to initiate processive transport *in vitro*, because the motor favored this isoform as an attachment point to dock onto the MTs (McKenney et al., 2016). Recent work now also demonstrated a role for the mouse tubulin glycylation enzymes. *in vitro* fertility assays showed that the lack of both *TTLL3* and *TTLL8* perturbed sperm motility causing male subfertility in mice. Structural analyses further suggested that loss of glycylation decreased axonemal dynein activity (Gadadhar et al., 2021).

A recent *in vivo* mouse study showed that hyperglutamylation of α-tubulin by TTLL1, but not β-tubulin, increased the overall (both anterograde and retrograde) motility of mitochondria, perturbed axonal transport, and led to neurodegeneration (Bodakuntla et al., 2021). Somewhat surprisingly, however, another study showed that the vesicular axonal transport was not affected by the absence of MT glutamylation in *Drosophila TTLL5* mutant

98 larvae (Devambez et al., 2017). Given these results and because the *Drosophila* gene is
99 also highly expressed in ovaries, we studied the *in vivo* role of *TTLL5* with a special focus on
100 the PTMs of the different α-tubulin isoforms in the ovary. This revealed that *TTLL5* is
101 essential for the normal glutamylation of the standard TBA1 and 3 isoforms. Surprisingly,
102 even in wild-type ovaries, the oogenesis-specific TBA4 was not glutamylated, suggesting
103 that this isoform may have evolved to produce MTs that contain regions that cannot be
104 glutamylated. We also found that *TTLL5* is required *in vivo* for the localization of mRNAs and
105 for cytoplasmic streaming, suggesting that these activities indeed depend on
106 polyglutamylation of α-tubulin. The transport of mitochondria in wing nerves is another
107 attractive system to study organelle transport (Vagnoni and Bullock, 2016) (Hollenbeck and
108 Saxton, 2005). We found the initiation of axonal transport of mitochondria in wing nerves
109 was strongly affected by lack of *TTLL5*. The overall motility and the processivity of the
110 mitochondrial transport also appeared to depend on α-tubulin glutamylation. Our work,
111 therefore, reveals the *in vivo* importance of glutamylation of specific α-tubulin isoforms.

112

113 **Results**

114 **Drosophila *TTLL5* is required for MT glutamylation of ovarian TBA1/3.**

115 To study the function of TTLL5, distinct *TTLL5* loss-of-function mutations were created and
116 characterized (**Fig. 1A**). The $TTLL5^{pBac}$ and $TTLL5^{Mi}$ mutant strains carry a piggyBac and a
117 Minos transposon, respectively, within the open reading frame of *TTLL5*. The $TTLL5^{MiEx}$
118 mutant was generated by imprecise excision of the Minos element, which caused the
119 formation of a premature stop codon at gene position 8,132 in the open reading frame
120 (codon position 392). An anti-TTLL5 antibody that cross-reacts with other proteins in ovarian
121 extracts also recognized a band at the size of TTLL5. This band turned out to be absent in
122 ovarian extracts prepared from the three *TTLL5* mutants, suggesting that they are protein
123 nulls for *TTLL5* or make only a truncated protein (**Fig. 1B**). A transgene containing the wild-
124 type *Drosophila TTLL5* sequence fused to the Venus fluorescent protein sequence under
125 UAS control (UASP-*Venus::TTLL5*) was also produced as a tool to rescue the phenotypes
126 produced by the *TTLL5* mutations and for overexpression studies (**Fig. 1A**).

127 To understand the effect of *TTLL5* on the glutamylation of the C-terminal tail of α-tubulins,
128 C-terminal peptides of the different α-tubulin isoforms were analyzed for post-translational
129 modifications by liquid chromatography-mass spectrometry (LC-MS). Proteins extracted from
130 ovaries were purified through SDS-PAGE. α-tubulin bands were cut out and digested with

131 the protease trypsin-N for MS. Because the resulting C-terminal peptides are identical
132 between the TBA1 and TBA3 isoforms, we will refer to them as TBA1/3 (**Fig. 2A**). Analyses
133 of wild-type ovarian extracts revealed that the general *Drosophila* isoforms TBA1/3, but not
134 the ovarian specific TBA4 isoform of α-tubulin showed glutamylation on the C-terminal tail of
135 α-tubulins (**Fig. 2A**, **S1**). For TBA1/3, side chain glutamylation was identified on all 4
136 glutamic acid residues in the tail region, Glu443, Glu445, Glu448, and Glu449, and the
137 longest side chains identified consisted of 3Es in wild-type ovaries **(Fig. 2A,2B)**. Determining
138 the frequency of C-terminal peptides containing the entire primary sequence and 0, 1, 2, and
139 3 Glu(E) modifications, we found that 62% of the peptides were modified in wild-type ovaries,
140 41% with 1E, 14% with 2Es, and 7% with 3Es **(Fig. 2C)**. On the other hand, no glutamylation
141 was observed in *TTLL5*^{pBac} and *TTLL5*^{MiEx} mutants. This clearly shows that *Drosophila*
142 *TTLL5* is essential for the side chain glutamylation of the C-terminal Glu443, Glu445, Glu448,
143 and Glu449 of TBA1/3.

144 We also measured the levels of monoglutamylation of α-tubulin by western blotting using
145 the GT335 antibody. This antibody reacts with the first glutamate on the glutamate side
146 chain even if it is polygutamylated (**Fig. 3A**) (Wolff et al., 1992). Note that the GT335
147 antibody does not reliably detect all mono glutamylated residues in *Drosophila* tubulins
148 because GT335 preferentially recognizes the first Glu attached to a Glu residue in an acidic
149 environment. In mice, the middle Glu in the sequence -G**E**E- of the C-terminal tail of α-
150 tubulin is such an "acidic" site. Once glutamylated, the branched Glu modification can be
151 recognized by GT335 (Bodakuntla et al., 2021). In contrast, in *Drosophila* α-tubulin, both
152 E443 and E445 in the sequence -G**E**G**E**G- are flanked by Glycines on both sides which does
153 not provide the acidic environment needed for efficient recognition by GT335. The GT335
154 signal may therefore mostly stem from the glutamylation on the consecutive Glu residues
155 E448 and E449 in the sequence -GA**EE**Y. On Western blots from wild-type extracts, the
156 GT335 antibody produced a band at the expected position and this band was reduced in all
157 *TTLL5* mutants. The GT335 signals were restored and even increased in some *TTLL5*
158 mutants upon overexpression of the rescue construct *Venus::TTLL5*, showing that the signal
159 is specific and can be used to monitor *TTLL5* activity **(Fig. 3B)**. We conclude that *TTLL5* is
160 required for monoglutamylation of α-tubulin.

161 The 1D5 antibody recognizes α-tubulin with an -XEE sequence at the C-terminal α-
162 carboxylate group (with X being a variable residue) (Rüdiger et al., 1999) **(Fig. 3A')**.
163 Therefore, in principle, all the Glu residues on E443, E445, E448, and E449 but also the C-
164 terminal Glu residues E448/449 can be recognized if they are not followed by another amino
165 acid (such as Tyr) at the α-carboxylate group. 1D5 does, therefore, not cross-react with C-

166 terminal Glu residues E448/449 in tyrosinated α-tubulin. Because *w* control ovaries showed
167 high 1D5 cross-reactivity with a polypeptide of the predicted size, this, therefore, indicates
168 the presence of glutamate side chains containing at least 2 glutamates and possibly de-
169 tyrosinated isoforms of α-tubulin (Gadadhar et al., 2017; Preston et al., 1979) **(Fig. 3B',**
170 **3B'')**. Consistent with the MS analysis, the *TTLL5* mutants showed a strongly reduced signal
171 with 1D5, indicating that loss of *TTLL5* function prevents normal polyglutamylation. The 1D5
172 signal was again restored in all *TTLL5* mutants upon expression of the rescue construct.
173 Overexpression of TTLL5 in *TTLL5*^{pBac} and *TTLL5*^{Mi} even produced a stronger 1D5 signal
174 and an up-shifted band, suggesting that α-tubulin gets hyper-glutamylated, maybe on
175 additional sites **(Fig. 3B')**. We also tested whether the overexpression of *TTLL5* in a wild-
176 type background affected polyglutamylation in the same way. Indeed, *UASP-Venus::TTLL5*
177 overexpression in ovaries led to hyper glutamylation as evident from the stronger signal and
178 the additional upshifted band **(Fig. 3C).** Glutamylation of β-tubulin was also evaluated by
179 using the antibody β-monoE which specifically recognizes monoglutamylation of the C-
180 terminal tail of β-tubulin (Bodakuntla et al., 2021) **(Fig. 3B'').** Results firstly showed a strong
181 signal of β-monoE in control ovaries, indicating that monoglutamylation occurred also on β-
182 tubulin in ovaries. However, the β-monoE levels were kept unchanged no matter whether
183 *TTLL5* was overexpressed or mutated. These results reveal that *TTLL5* is essential for the
184 glutamylation of MTs in the ovary, acting specifically on α-tubulin but not on the β- tubulin
185 subunit. It also suggests that TTLL5 levels are usually limiting in ovaries.

186 Most of the murine TTLL5 residues involved in α-tubulin glutamylation (van Dijk et al.,
187 2007) are conserved in *Drosophila* TTLL5 **(Table 1)**. Two are known to be important for the
188 general enzymatic activity of TTLLs and two for the interaction with the C-terminal domain of
189 α-tubulin **(Fig. 3D)**. To find out whether these residues are indeed needed *in vivo* for the
190 enzymatic activity of *Drosophila TTLL5 towards* TBA1/3, we used CRISPR/Cas9 to mutate
191 the conserved codons in *Drosophila TTLL5. Drosophila* TTLL5 residues K282 and E517*,*
192 respectively, correspond to mouse K131 and E336*,* respectively*.* They directly interact with
193 ADP/ATP and thus affect general TTLL5 enzymatic activity (van Dijk et al., 2007). TTLL5^{R339}
194 corresponds to mouse TTLL5^{R188}*,* which is important for TTLL5's glutamylation activity.
195 MmTTLL5^{R188} resides in the β6-7 loop, which forms a salt-bridge interaction with the C-
196 terminal tail of α-tubulin and orients it towards the ATP/ADP-binding site (van Dijk et al.,
197 2007). Glutamylation of α-tubulin was impaired in all these *TTLL5* mutants where the
198 conserved residue was replaced **(Fig. 3E)**. Since these mutations did not abolish the stability
199 of the corresponding mutant protein (**Fig. S2**), our results revealed the importance of E517,
200 K282, and R399 of *Drosophila* TTLL5 for glutamylation. Because almost all active site
201 residues of human TTL (Prota et al., 2013; van Dijk et al., 2007) are also conserved between

202 mammalian and *Drosophila* TTLL5 **(Table 2)**, we also mutated the *Drosophila TTLL5*^{P522}
203 codon corresponding to human *TTL*^{P336} (and mouse *TTLL5*^{P371}), which is required for
204 anchoring TTL to α-tubulin by forming hydrogen bonds with C-terminal tail residues of α-
205 tubulin (Prota et al., 2013). However, the importance of *TTLL5*^{P371} has not been reported in
206 mammalian systems. Somewhat surprisingly, in *Drosophila*, P522 turned out to be essential
207 for glutamylation as well, revealing P522 as a novel important residue for the glutamylation
208 function of TTLL5.

209 **Other PTMs of the C-terminal tail of ovarian α-tubulin**

210 Our MS results also detected glycylated C-terminal α-tubulin peptides in ovarian samples.
211 The glycylations were observed on the C-terminal tail of the *Drosophila* ovarian TBA1/3
212 isoforms, but not on TBA4 **(Fig. S3A, S3B)**. Up to 2 glycines were detected mostly on
213 Glu443, Glu445, Glu448, or Glu449 of TBA1/3. The frequency of C-terminal peptides
214 containing Gly (G) modifications was similar or somewhat higher in *TTLL5* mutants
215 compared to the wild-type control **(Fig. S3C)**, suggesting that *TTLL5* is not needed for this
216 modification or even counteracts it.

217 Western blotting showed no or only minor changes in tyrosinated α-tubulin levels in any of
218 the null or CRISPR/Cas9 generated point mutants, and *TTLL5* overexpression did also not
219 affect these levels **(Fig. 3B, 3C, 3E).** TTLL5 levels, therefore, do not appear to affect levels
220 of tyrosinated α-tubulin in ovaries.

221 **Effect of *TTLL5* on Kinesin-1 dependent refinement of posterior localization of Staufen**

222 *osk* mRNA localization, combined with translation control, is important for targeting Osk
223 protein expression to its proper posterior compartment in the cell (Suter, 2018; Weil, 2014).
224 Staufen is a ribonucleoprotein (RNP) that associates with *osk* mRNA during *osk* mRNA
225 localization. The localization of Staufen/*osk* mRNA requires the dynein/dynactin mediated
226 minus-end transport machinery in the early stages of oogenesis. Subsequently, the
227 Staufen/*osk* mRNA becomes localized to the posterior of the oocyte from mid to late stages
228 of oogenesis and this particular Staufen/*osk* mRNA localization phase within the oocyte
229 depends on a kinesin driven process including Kinesin-1 based active transport and
230 ooplasmic streaming in stage 10B (S10B) oocytes (Kato and Nakamura, 2012) (Lu et al.,
231 2018) (Brendza et al., 2000) (Zimyanin et al., 2008). To find out whether *TTLL5* contributes
232 to this process, we studied the role of *TTLL5* in dynein and kinesin transport by analyzing the
233 localization of Staufen in ovaries lacking functional TTLL5.

234 An established method to quantify the localization of Staufen to the posterior cortex is to
235 measure the length of the posterior Staufen crescent along the cortex (Lu et al., 2016). A
236 shorter crescent is a sign of better, tighter localization. We found that the length of the
237 posterior Staufen crescent was significantly increased in *TTLL5* null and *TTLL5* point mutant
238 ovaries compared to control ovaries (**Fig. 4A', 4A''', 4B'-B'')**. Furthermore, Z-stack images
239 revealed a more diffusely spread Staufen signal in all *TTLL5* mutants, although this varied
240 more between different samples **(Fig. 4A', 4B')**. The increased length of the crescent was
241 fully reversed to the normal length in all UAS-*Venus::TTLL5* rescued strains **(Fig. 4A''-A''')**.
242 We also analyzed the distribution of Venus::TTLL5 during oogenesis. Antibody staining
243 suggested that Venus::TTLL5 strongly accumulated in the oocyte and especially along the
244 cortex **(Fig. 4A'')**. In conclusion, the posterior localization refinement of Staufen in S10B
245 oocytes requires *TTLL5* and, because the point mutation specifically blocks the enzymatic
246 activity of TTLL5, it appears that the proper localization requires glutamylation of tubulin.

247 To test if *TTLL5* is also required by the dynein/dynactin machinery and the Staufen/*osk*
248 mRNA transport during previtellogenic stages of oogenesis, we also imaged the localization
249 of Staufen and Bicaudal-D (BicD) protein in early stages. BicD is the linker that couples
250 diverse cargos to the dynein/dynactin motor and is thus a good marker to evaluate dynein
251 transport function (Claussen and Suter, 2005). Both BicD and Staufen showed similar
252 localization patterns during early oogenesis in *TTLL5* mutant and control ovaries **(Fig. 4C-**
253 **C')**. The expression of BicD was not affected by the levels of TTLL5 as assessed by
254 Western blotting (**Fig. 4D**, **Fig. S4**). These results indicated that in ovaries, kinesin-
255 dependent localization processes require *TTLL5* whereas the dynein-dependent transport
256 does not appear to depend on *TTLL5*.

257

258 **Kinesin-1 dependent ooplasmic streaming in stage 10B oocytes requires *TTLL5***

259 Ooplasmic streaming is a bulk movement of the oocyte cytoplasm that circulates and
260 distributes mRNAs and proteins in the oocyte, including the Staufen/*osk* mRNA RNPs. It
261 allows these mRNA and proteins to reach their intended position where they become
262 anchored. Slow and nondirectional flows initiate at stages 8–9 and are followed by rapid and
263 circular streaming at S10B (Lu et al., 2016). Kinesin-1-dependent microtubule sliding is
264 critical for this fast ooplasmic streaming (Lu et al., 2016). The kinesin-dependent final
265 posterior localization of Staufen in S10B oocytes depends on this process and *TTLL5*. Aside
266 from this, the TTLL5 protein was present in the cortical region of the oocyte **(Fig. 4A")**, the

267 region where the microtubule sliding occurs (Lu et al., 2018). We thus wanted to find out if
268 *TTLL5* contributes to an efficient kinesin-dependent sliding that drives ooplasmic streaming.

269 We firstly examined the levels of Kinesin-1 and found that they were neither affected in
270 *TTLL5* mutant ovaries nor in ovaries overexpressing *Venus::TTLL5* (**Fig. 5A, Fig. S4**). To
271 test if *TTLL5* is needed for ooplasmic streaming, we followed this process in real time by
272 measuring vesicle movement in DIC time-lapse movies (**Mov. S1-S4**). We then tracked the
273 movement of the vesicles along the cortex region where microtubule sliding occurs (**Fig. 5B**).
274 The velocity of the tacked vesicles was not to be affected in *TTLL5* mutant ovaries (**Fig. 5C**).
275 However, the analysis of the kymographs of these tracked vesicles showed that while control
276 ovaries have a normal streaming pattern with vesicles moving with a flow direction parallel to
277 the cortex, $TTLL5^{MiEx}$ and $TTLL5^{E517A}$ mutant ovaries displayed a disordered streaming
278 pattern (**Fig. 5D**). The normal streaming pattern was restored in $TTLL5^{MiEx}$ ovaries
279 expressing a *Venus::TTLL5* rescue construct. Because the point mutation specifically blocks
280 the enzymatic activity of TTLL5, our results suggest that TTLL5 is important to control the
281 directionality of the fast ooplasmic streaming through its role in MT glutamylation.

282 **Transport of mitochondria in neurons depends on the glutamylation activity of *TTLL5***

283 Previous studies in *Drosophila* reported that *TTLL5* is required for the initiation of α-tubulin
284 glutamylation in the nervous system (Devambez et al., 2017). However, the absence of α-
285 tubulin glutamylation seemed not to be detrimental to the tested nervous system functions in
286 *Drosophila* (Devambez et al., 2017). To study neuronal transport in the peripheral nervous
287 system, the wing nerves are an attractive system to monitor organelle transport such as the
288 movement of mitochondria (Vagnoni and Bullock, 2016) (Hollenbeck and Saxton, 2005).
289 Consistent with a previous report, we found that in extracts from a mixture of heads and
290 wings, α-tubulin was glutamylated and this PTM depended on the enzymatic activity of
291 TTLL5 (**Fig. 6A)**; (Devambez et al., 2017). This suggests that the wing nerve could be a
292 suitable system for this test.

293 To study if neuronal transport of mitochondria in wing neurons depends on glutamylation of
294 α-tubulin, we tracked the movement of GFP-labelled mitochondria (Mito::GFP) in selected
295 areas of both the L1 and L3 wing veins of freshly eclosed flies (**Fig. 6B**). Time-laps videos of
296 Mito::GFP movement in the L1 and L3 veins, respectively, are shown in **Mov. S5** and **Mov.**
297 **S6**, respectively. Motile mitochondria were manually tracked using the Fiji MTrackJ plugin
298 (**Fig. 6C**). Movies and still images clearly showed a decrease of motile mitochondria in the
299 region close to the arch of the L1 vein and no transported mitochondria in the L3 vein of the
300 $TTLL5^{E517A}$ mutant, pointing to the importance of the enzymatic activity of TTLL5 for proper

301 transport. For quantitative analysis, the ratio of motile particles was calculated based on the
302 values divided by total particles from 3 wings of each genotype (**Fig. 6D**). The total particles
303 include all the static and transporting ones which were counted based on the signal from one
304 chosen still image. Quantifications showed, firstly, that the total number of particles in the L1
305 vein (384) was twice as high as in the L3 vein (186). This is likely because the L1 vein
306 contains more neurons than the L3 (Vagnoni and Bullock, 2016). Secondly, however, in wild-
307 type wings, the fraction of motile mitochondria is higher (24%) in L3 veins than in L1 veins
308 (7.8%). This might be because compared to the L3 vein, which consists mainly of axons
309 (Vagnoni and Bullock, 2016) (**Fig. S5**), the region close to the arch of the L1 vein contained
310 not only axons but also several cell bodies and dendrites (Vagnoni and Bullock, 2016) (**Fig.**
311 **S5**). Mitochondria in dendrites are longer than those in axons (Chang et al., 2006). The
312 longer mitochondria are less motile than the short ones (Misgeld et al., 2007). The large
313 number of less motile mitochondria in cell bodies and dendrites "diluted" the motile
314 mitochondria ratio in L1 veins. Because axons are easily distinguishable in the L3 vein, the
315 region of L3 seemed to be a better choice for axonal transport studies than the one in the L1
316 vein. The quantification of the motile ratio in the *TTLL5*^{E517A} mutant showed no motile
317 mitochondria in the L3 vein of the *TTLL5*^{E517A} mutant (**Fig. 6D**), strongly indicating that
318 *TTLL5* is required for the initiation of axonal transport of mitochondria. Apart from this, the
319 quantification of the motile ratio in the L1 showed a drop from 7.8% (plus-end 5.3% and
320 minus-end 2.5%) in the control to 1.9% in *TTLL5*^{E517A} mutant wings (plus-end 1.5% and
321 minus-end 0.4%) (**Fig. 6D** and **Table 3**). These results reveal the importance of the
322 enzymatic activity of *TTLL5* for *in vivo* mitochondrial transport in wing nerves.

323 Because no motile mitochondria were found in the L3 region, we evaluated other
324 transport parameters in the L1 region. The *Drosophila* sensory neurons contain axons with
325 plus-end-out MTs and dendrites with minus-end-out MTs (Stone et al., 2008; Zheng et al.,
326 2008). Though the L1 region is enriched in a mix of axons, dendrites, and cell bodies, the
327 direction of the organelle transport can still be established. The mitochondria transported
328 towards the thorax of a fly move by plus-end transport, driven by kinesin, whereas
329 mitochondria transported away from the thorax are transported by dynein. We examined the
330 parameters of running patterns, trafficking length, and velocity of mitochondrial movement in
331 region L1. The start of a run was chosen at the time point when a motile particle began to
332 move from a stationary position, and the stop of a run was defined when the particle stopped
333 moving. Pausing of a run was called when the particle moved at a rate lower than 0.2 μm/s.
334 Particles with a speed higher than 0.2 μm/s were considered as "trafficking". A schematic
335 running pattern is shown in **Fig. 6E.** Bidirectionally moving particles were seen only very
336 rarely in our case. In these cases, they usually moved a short distance towards one direction

337 and suddenly turned back and ran in the opposite direction. For the plus-end transport
338 (**Table 3)**, the average total duration of a running time showed no significant difference
339 between controls (92s) and *TTLL5* mutants (98s). As well, no significant difference in the
340 mean velocity of the tracked mitochondria was observed between controls (0.37 μm/s), and
341 *TTLL5*^{E517A} mutants (0.36 μm/s). However, the average pausing time ratio in *TTLL5*^{E517A}
342 (63%) showed a decrease compared to the control (74%), suggesting that α-tubulin
343 glutamylation was required for attaching and holding or stopping mitochondria during their
344 whole "run" along MTs (see **Fig. 6E**). Consistent with this observation, mitochondria in
345 *TTLL5*^{E517A} moved longer distances (12μm) than the mitochondria observed in the controls
346 (7μm). Even though our research focused on the plus-end transport, preliminary numbers for
347 the minus-end transport suggest that the motile frequency, total duration and pausing time
348 ratio might decrease in *TTLL5*^{E517A}, too (**Table 3**). However, the small numbers for
349 *TTLL5*^{E517A} do not allow to conclude this.

350 It appears that two different mechanisms might be involved between the start and the
351 ongoing transport of individual mitochondria. At the first step, the lack of glutamylation
352 hinders the initiation of the axonal transport of mitochondria, indicating that initiation of
353 processive axonal transport heavily depends on glutamylation. Once mitochondria have
354 started to move, the lack of α-tubulin glutamylation increases the plus-end trafficking time
355 and trafficking length of the mitochondria in a region of the wing nerve that contains axons,
356 dendrites and cell bodies, indicating that glutamylation is also needed for holding or
357 anchoring mitochondria on the MTs during trafficking in neurons. Altogether, these results
358 demonstrated the role of α-tubulin glutamylation for the efficient mitochondrial transport in
359 wing nerves.

360

361 **Discussion**

362 Both western blotting and MS results from wild-type and mutant *Drosophila* revealed that
363 *TTLL5* is essential for polyglutamylation of α-tubulin in ovaries. The complete lack of even
364 monoglutamylated α-tubulin tails in the presumptive null mutants of *TTLL5* strongly suggests
365 a requirement for TTLL5 for adding the first branching Glu to the Glu side chains in the C-
366 term. The requirement for adding the first Glu could also account for the lack of
367 polyglutamylation in the mutants. This result is also consistent with results from HeLa cells
368 and the *Drosophil*a nervous system (Devambez et al., 2017; van Dijk et al., 2007). Further
369 MS results indicated that *TTLL5* specifically functions to glutamylate the TBA1/3, but not the
370 TBA4 isoforms of α-tubulin. Up to three Glu residues were found added to the positions

371 E443/E445/E448/E449 of TBA1/3 (**Fig. 2A, 2B**). Even though TBA4 is an ovarian-specific
372 isoform, our MS analysis showed a lower amount of TBA4 peptides than TBA1/3 peptides
373 (**Table S3**), suggesting that it accumulated at a lower level in ovaries. The fact that we could
374 not find any glutamylation in TBA4 could indicate that this isoform evolved because the
375 ovary has a need for non-glutamylated α-tubulins. As we could show here, glutamylation
376 plays an important role in kinesin-driven processes. The evolutionary appearance of a non-
377 glutamylatable tubulin isoform may indicate that this tissue has a need for special
378 microtubules that favour specifically other MT motor transport, and this could be achieved by
379 setting up MTs or MT regions that are preferentially being used for dynein-driven transport.

380 Our MS analysis revealed that polyglycylation of α-tubulin also takes place in the ovarian
381 tissue and that glycylation modifies the same sites in the C-terminal domain as
382 polyglutamylation does, the side chains of the Glutamic acid residues. Because glycylation is
383 still seen in the *TTLL5* mutants, TTLL5 does not seem to be the enzyme for this reaction,
384 and glutamylation of one site is not a prerequisite for glycylation of another site. It would now
385 be interesting to find out whether glycylation even serves to prevent glutamylation or to
386 compete with it and whether this is used as another level of control of microtubule activity. A
387 preliminary analysis of glycylation in the *TTLL5* mutants suggests that this might be possible
388 (**Fig. S3C**). In *Tetrahymena* such a competition has been described because there, Glutamic
389 acid and Glycine ligases competed for the same sites or affected each other by sterically
390 blocking adjacent sites of tubulins (Redeker et al., 2005; Wloga et al., 2009). Only a
391 surprisingly small fraction of the *TTLL* family is expressed in *Drosophila* ovaries according to
392 Flybase. Aside from *TTLL5*, we only found evidence for the expression of *TTLL4A* and
393 *TTLL12* **(Table S2)**. Our genetic analysis of *TTLL5* showed that it is not required for
394 glycylation. The predicted mouse homolog of the *Drosophila TTLL4A* was found to
395 glutamylate β-tubulin (Mahalingan et al., 2020), suggesting that this isoform could be the one
396 required for β-tubulin glutamylation in ovaries. The function of the predicted homolog of
397 *Drosophila TTLL12* in mammals was poorly studied and the core TTL domain of mouse
398 TTLL12 is less conserved than other mouse E- and G- ligases of the TTLL family (van Dijk et
399 al., 2007). It is, therefore, not clear yet which enzyme performs the polyglycylation of α-
400 tubulin in *Drosophila* ovaries.

401 The ooplasmic streaming process is required for the posterior localization of Staufen/*osk*
402 mRNA and is mediated by an MT-sliding mechanism (Lu et al., 2016). This MT-sliding, which
403 is an essential step for normal oogenesis, involves the sliding between the cortically
404 anchored microtubules and the free cytoplasmic microtubules that are located close to the
405 cortex. This sliding between the two classes of microtubules is Kinesin-1 dependent. Our

406 data show that *TTLL5* is needed for normal oocyte cytoplasmic streaming and for the
407 posterior localization of Staufen/*osk mRNA*, suggesting that it affects these processes
408 through a role in kinesin-1 dependent MT sliding.

409 It is worth pointing out that *in vitro* studies demonstrated that the artificial tethering of
410 glutamyl peptides to the side chains of both α- and β-tubulin increased the run length of
411 Kinesin-1 on tubulins (Sirajuddin et al., 2014). *Drosophila TTLL5* is essential for
412 glutamylation of α-tubulin but not for β-tubulin. These results, first of all, provide the best
413 evidence yet that *TTLL5* mediated glutamylation of α-tubulin plays an important role in
414 Kinesin-1 driven processes *in vivo*. However, the phenotypes including reduced ooplasmic
415 streaming and Staufen localization observed in *TTLL5* mutants were not as severe as the
416 ones that arose when Kinesin heavy chain (KHC) was not functional (Lu et al., 2016).
417 Besides, in the wing nerve experiment, though initiation of mitochondria was heavily
418 dependent on the glutamylation of α-tubulin, there are still some particles which started to be
419 transported in *TTLL5* mutants. It therefore seems possible that α-tubulin glutamylation is not
420 absolutely required for transport initiation and this poses the interesting novel question
421 whether these Kinesin-1 dependent processes can still operate if β-tubulin is glutamylated.

422 In *KHC* mutants, there is an overall decrease in anterograde as well as dynein-driven
423 retrograde transport of mitochondria in *Drosophila* larval motor axons (Pilling et al., 2006).
424 We observed a similar loss of motile mitochondria in the axon-rich region in the *TTLL5*^{E517A}
425 mutant wing (**Fig. 6C, 6D**). Because both previous studies (Devambez et al., 2017) and our
426 data (**Fig. 6A**) showed that *TTLL5* was required for α-tubulin glutamylation in the nervous
427 system, all these results suggested that α-tubulin glutamylation is a crucial factor for the
428 Kinesin-1 mediated initiation of mitochondrial transported in axons.

429 By analyzing the dynamics of the few motile mitochondria observed in L1 veins, we found
430 that in the absence of glutamylation, the plus-end mitochondria can run longer distances with
431 shorter pausing times. (**Fig. 6G**). Interestingly, a recent study linked the reduced trafficking
432 time of mitochondria during axonal transport to neurodegeneration in mice and this was
433 caused by hyperglutamylation of α-tubulin but not β-tubulin (Bodakuntla et al., 2021). It thus
434 strongly indicated the glutamylation of α-tubulin causes the halting of the ongoing transport
435 of single mitochondria *in vivo*. Because the orientation of the MTs in the *Drosophila* wing
436 neurons is unidirectional and the plus-end transport of mitochondria was affected in the
437 absence of the glutamylation of α-tubulin, we now learned that glutamylation is at least
438 needed for the Kinesin-1-based transport.

439 Several mechanisms have been proposed to stop mitochondrial transport in neurons. For
440 instance, tethering mitochondria to the actin cytoskeleton (Pathak et al., 2010), blocking the
441 binding of Kinesin-1 to MTs by increasing Ca^{2+} (Wang and Schwarz, 2009), abolishing the
442 interaction between Kinesin-1 and mitochondria by degrading one of the linker proteins
443 (Miro; Wang et al., 2011), or possibly traffic jam. We here provided *in vivo* evidence that
444 glutamylation of MTs is an important regulatory mechanism that contributes to the
445 sophisticated neuronal mitochondrial transport system.

446

447 **Materials and methods**

448

449 **Drosophila genetics**

450 The fly stocks used in this study, MattubGal4 (7062), *TTLL5*^{pBac} (16140), *TTLL5*^{Mi} (32800),
451 and *Df(3R)BSC679* (26531), were obtained from the Bloomington Drosophila stock center.
452 The *TTLL5*^{MiEx} mutation was made by imprecise excision of the Minos element, which left a 3
453 base insertion (CTA) that introduces a premature stop codon at genomic position 8,132 in
454 the open reading frame (polypeptide position 392). The different *TTLL5* point mutations were
455 generated by CRISPR/Cas9. The two Drosophila stocks used for *TTLL5* gene editing, *y[1]*
456 *M{w[+mC]=nos-Cas9.P}ZH-2A w[*]* and *y[1] v[1] P{y[+t7.7]=nos-phiC31\int.NLS};*
457 *P{y[+t7.7]=CaryP} attP40* were obtained from the Bloomington Drosophila Stock Center
458 (54591) (Port et al., 2014) and (25709), respectively. Target sequences near the K131, R339
459 R376, and E517 codons were selected to introduce INDELs and the following point
460 mutations: K131A, R339A (b6-7 loop), R376A, and E517A. Phosphorylated and annealed
461 primers (Table S1A) needed to construct the corresponding coding sequences for a single
462 guide RNA (sgRNA) were each cloned into the BbsI site of *pCFD5* according to the protocol
463 published on www.crisprflydesign.org. After amplification of the vector in XL1 blue cells, the
464 plasmids were sequenced to verify correct assembly. Subsequently, they were injected into
465 *attP40* embryos. TTLL5-guide stocks with integrated genes encoding sgRNAs were
466 established *(=v; attP40{v*$^{+}$*, TTLL5-guide}/CyO*). To obtain INDELs for TTLL5, a three-
467 generation crossing schema was set up. Firstly, *nos-cas9* virgins were crossed with males
468 from the different TTLL5-guide stocks. Secondly, the subsequent single male progeny was
469 crossed with *w; Ly/TM3, Sb* virgins. Thirdly, resulting single *TM3, Sb* males were again
470 crossed with *w; Ly/TM3, Sb* virgins to establish the stocks. The nature of the mutated *TTLL5*
471 gene in each stock was determined by sequencing. To introduce specific point mutations in
472 the *TTLL5* gene, embryos from a cross with *y w {w*$^{+}$*, nos-cas9}* virgins and TTLL5-guide
473 males were injected with the appropriate template (**Table S1B).** The resulting individual adult
474 males were crossed with *w; Ly / TM3, Sb* virgins, and stocks were established. The
475 presence of a mutated *TTLL5* gene was confirmed by restriction digestion and subsequent
476 sequencing. All the *TTLL5* alleles were crossed to *Df(3R)BSC679* to test the effect of the
477 *TTLL5* mutations in hemizygous animals. The *UASp-venus::TTLL5* DNA construct was
478 made from the *TTLL5* cDNA amplified by PCR (forward primer: 5′ -
479 GTTCAGATCTATGCCTTCTTCATTGTGTG -3′; reverse primer: 5′ -
480 GAGTCATTCTAGAGCTTCATAGAAATACCTTCTCC- 3′) and inserted into the *pUASP-*
481 *venus* vector via Xba I/Bgl II ligation. DNA was inserted into the *attP-58A* landing platform

482 (24484) to generate the transgenetic *UASp-venus::TTLL5* fly strain. *ApplGal4* and *UAS-*
483 *mito::GFP* were kindly provided by Simon Bullock's group (Vagnoni et al., 2016).

484 **Western blotting**

485 Western blotting performed with ovarian extracts was carried out with 10-20 pairs of ovaries
486 for each genotype. Newly hatched females of the indicated genotypes were collected and
487 crossed with *w* males in fresh vials with ample yeast food for two days. Fully developed
488 ovaries were then dissected and collected. To analyze neuronal samples, a mixture of head
489 and wing tissue from 30 flies was collected for each genotype. The samples were directly
490 lysed in Laemmli buffer, boiled at 95°C for 10 min, and analyzed by SDS-PAGE.
491 Chemiluminescence detection was done with the Amersham imager 600 (GE healthcare).
492 The following primary antibodies were used: mouse 1D5 (1:500, Synaptic System), mouse
493 GT335 (1:200, Adipogen), mouse DM1A (1:1,000, Sigma), mouse tyrosinated α-tubulin
494 (1:1,000, Sigma), rabbit GFP (1:2,000, Sigma), rabbit GAPDH (1:1,000, GeneTex), rabbit
495 TTLL5 (1:500, GenScript), mouse BicD (1B11 plus 4C2, 1:5) (Suter and Steward, 1991),
496 rabbit KHC (1:1,000, cytoskeleton), rabbit β-monoE (1:1,000) (Bodakuntla et al., 2021).
497 Secondary antibodies were HRP-linked goat anti-mouse (1:1,0000, GE Healthcare) and
498 HRP-linked goat anti-rabbit (1:10,000, GE Healthcare). Antibodies were incubated in 5%
499 non-fat milk PBST (PBS with 0.1 % Triton X-100) and washed with PBST.

500 **Immunoprecipitations (IPs) and Mass Spectrometry**

501 Proteins were extracted from the ovaries of 100 3-day-old, well-fed females of each
502 genotype, crossed to wild-type males, and proteins were immunoprecipitated with an α-
503 tubulin antibody (Sigma) bound to G-protein coupled magnetic beads. Samples (ligated with
504 beads) were boiled and run on SDS-PAGE. These were then stained with Coomassie Blue.
505 The gel pieces containing the α-tubulin region were cut, alkylated, and digested by trypsin N
506 (ProtiFi) for 3 hours at 55°C. C-terminal peptides of α-tubulin were analyzed by liquid
507 chromatography (LC)-MS/MS (PROXEON coupled to a QExactive mass spectrometer,
508 Thermo Fisher Scientific). Samples were searched against the UniProtKB Drosophila
509 database using Pipeline, PEAKS, Easyprot and MSfragger as search engines. Peptides
510 were shown by PSM value (peptide spectrum match). To avoid repetition of total PSM
511 quantification, we searched only for one type of PTM in an analysis per time. Total PSM
512 indicates the sum of PSMs of primary C-terminal peptides with either glutamylation or
513 glycylation modifications, or non-modified peptides.

514 **Ooplasmic streaming in live oocytes**

515 Three days old females were kept together with wild-type males under non-crowding
516 conditions at 25°C on food containing dry yeast. The determination of ooplasmic streaming
517 was based on the method of Lu and colleagues (Lu et al., 2016). Ovaries were directly
518 dissected in 10S halocarbon oil (VWR) and eggs were teased apart in the oil drop on a
519 24×50 mm coverslips (VWR). Living stage 10B oocytes were directly observed and imaged
520 with the 60×1.4 N.A. oil immersion objective on a Nikon W1 LIPSI spinning disk with a
521 2x Photometrics Prime BSI CMOS camera. Time-lapse images were acquired every 2s for 2
522 min under bright-field (BF) controlled by Nikon Elements software. Flow tracks were
523 generated by kymographs using Fiji (Schindelin et al., 2012) plugin Multi Kymograph (https://
524 imagej.net/ Multi _Kymograph). The velocity of 100-200 particles/ooplasm was tracked using
525 Analysis > Distribution of Speed (Track-Based) by DiaTrack 3.05 (Vallotton and Olivier,
526 2013), with a maximum jumping distance of 3.24 μm/s. The datasets were exported to Excel,
527 where the mean velocities of each ooplasm were analyzed. Then the velocities of different
528 ooplasms from different genotypes were shown as means ± S.E.M. by Prism 5 software
529 (GraphPad).

530 **Immunostaining and confocal microscopy**

531 Ovaries were dissected in 1× PBS and fixed in buffer (200 μl 4% formaldehyde (Sigma), 600
532 ul Heptane (Merck Millipore), 20 ul DMSO (Sigma) for each group) for 20 min. Samples were
533 blocked in PBST (PBS with 0.1 % Tween 20) with 5% non-fat milk powder and 0.1 % Triton
534 X-100 for 1 h. Ovaries were incubated with rabbit anti-Staufen (1:2,000) (St Johnston et al.,
535 1991), mouse anti-BicD (1B11 plus 4C2, 1:5) (Suter and Steward, 1991) and rabbit anti-GFP
536 (1:200, Sigma) antibodies at 4°C overnight, and incubated with secondary Alexa Fluor goat
537 anti-mouse 647 (1:400, Jackson ImmonoResearch) and Alexa Fluor goat anti-rabbit 488
538 (1:400, Life technologies Thermo Fischer) at room temperature for 3 h. DNA and nuclei were
539 stained using Hoechst 33528 (Thermo Fischer Scientific) for 10 min. Mounted samples were
540 imaged with a Leica TCS SP8 confocal microscope equipped with a 63×1.40 oil lens and
541 controlled by the Las X software (Leica). Images of single focal planes and 12 μm Z
542 projection were acquired. The crescent length of Staufen was processed by the Fuji
543 segmented line tool based on the single plane. The data were shown as means ± S.E.M. by
544 Prism 5 (GraphPad software). The statistical significance was determined by an unpaired
545 two-tailed non-parametric t-test (Mann-Whitney test).

546 **Mitochondrial transport in Drosophila wing neurons**

547 Mitochondrial transport in Drosophila wing neurons was tracked as described (Vagnoni and
548 Bullock, 2016). In brief, newly eclosing flies were anesthetized with CO_2 and immobilized in

549 a custom-built chamber formed of two No.1.5 24×50 mm coverslips (VWR). Imaging of
550 wings was performed with a Nikon W1 LIPSI spinning disk microscope equipped with a 2x
551 Photometrics Prime BSI CMOS camera and a 60×1.4 N.A. oil immersion lens. Time-lapse
552 video of a single focal plane was acquired with an acquisition rate of 0.5 frame/s for 3 min for
553 Mito::GFP using a 488 nm laser.

554 Quantification of the movements was performed in Fiji. A region close to the axonal tract of
555 the wing arch of the L1 vein and a region of the L3 vein were selected and straightened with
556 the Straighten plugin (Eva Kocsis, NIH, MD). For each "run", the total run distance of more
557 than 2 μm was defined as "transported or motile mitochondria". To exclude the oscillatory
558 movements of mitochondria, a minimal instant velocity between each frame was defined at
559 0.2 μm/s. Transported mitochondria were manually marked with MTrackJ plugin (Meijering
560 et al., 2012) and tracked by the manual tracking plugin (Fabrice Cordelières, Institute Curie,
561 France). The total number of mitochondria was counted from a single frame using the
562 "Analyze particle" function of Fiji. Run length, velocity values, and total running & pausing
563 times were exported into Excel for analysis. The data were shown as means ± S.E.M. by
564 Prism 5 (GraphPad). The statistical significance was determined with the student's t-test.

565 **Sequence alignment**

566 Sequences were aligned by CLC Sequence Viewer 8.0 software (Qiagen). The UniProtKB
567 accession numbers are as follows: *HsTTL*: Q8NG68; *HsTTLL5*: Q6EMB2; *MmTTLL5*:
568 Q8CHB8; *DmTTLL5*: Q9VBX5;

569 **Acknowledgments**

570 We thank Carsten Janke (Institute Curie, France) for anti-β-monoE antibodies, Simon L.
571 Bullock (Cambridge, UK) for *ApplGal4* and *UAS-mito::GFP* fly lines, Michel Steinmetz (Paul
572 Scherrer Institute, Switzerland), and the Janke laboratory members for discussions, and
573 suggestions. We also thank the Mass Spectrometry center (University of Bern, Switzerland)
574 members Sophie Braga Lagache and Natasha Buchs for performing the MS experiments,
575 and Manfred Heller and Anne-Christine Uldry for peptide analysis and discussion of the
576 results.

577

578 **Support**

This work was financially supported by the project grants 31003A_173188 and 310030_205075 from the Swiss National Science Foundation (SNF; https://www.snf.ch/en) to B.S. Equipment support was by an equipment grant from SNF (316030_150824) to B.S. and by the University of Bern (https://www.unibe.ch). Additional salary and material support were received from the University of Bern (https://www.unibe.ch) to B.S. The funders had no role in the study design, data collection, and analysis, decision to publish, or preparation of the manuscript.

The authors declare no competing financial interests.

Author contributions: Mengjing Bao, Beat Suter, and Maria Paula Vazquez-Pianzola conceived the project and designed the experiments. Mengjing Bao, Beat Suter, Ruth Dörig, and Dirk Beuchle performed the experiments and analyzed the data; Mengjing Bao and Beat Suter wrote the manuscript.

Reference

Arce, C.A., J.A. Rodriguez, H.S. Barra, and R. Caputo. 1975. Incorporation of L-tyrosine, L-phenylalanine and L-3,4-dihydroxyphenylalanine as single units into rat brain tubulin. *Eur J Biochem*. 59:145-149.

Bodakuntla, S., X. Yuan, M. Genova, S. Gadadhar, S. Leboucher, M.C. Birling, D. Klein, R. Martini, C. Janke, and M.M. Magiera. 2021. Distinct roles of α- and β-tubulin polyglutamylation in controlling axonal transport and in neurodegeneration. *EMBO J*. 40:e108498.

Brendza, R.P., L.R. Serbus, J.B. Duffy, and W.M. Saxton. 2000. A function for kinesin I in the posterior transport of oskar mRNA and Staufen protein. *Science*. 289:2120-2122.

Chang, D.T., A.S. Honick, and I.J. Reynolds. 2006. Mitochondrial trafficking to synapses in cultured primary cortical neurons. *J Neurosci*. 26:7035-7045.

Claussen, M., and B. Suter. 2005. BicD-dependent localization processes: from Drosophilia development to human cell biology. *Ann Anat*. 187:539-553.

Devambez, I., J. van Dijk, S. Benlefki, S. Layalle, Y. Grau, K. Rogowski, M.L. Parmentier, and L. Soustelle. 2017. Identification of DmTTLL5 as a Major Tubulin Glutamylase in the Drosophila Nervous System. *Sci Rep*. 7:16254.

Eddé, B., J. Rossier, J.P. Le Caer, E. Desbruyères, F. Gros, and P. Denoulet. 1990. Posttranslational glutamylation of alpha-tubulin. *Science*. 247:83-85.

611 Gadadhar, S., G. Alvarez Viar, J.N. Hansen, A. Gong, A. Kostarev, C. Ialy-Radio, S.
612 Leboucher, M. Whitfield, A. Ziyyat, A. Touré, L. Alvarez, G. Pigino, and C. Janke.
613 2021. Tubulin glycylation controls axonemal dynein activity, flagellar beat, and male
614 fertility. *Science*. 371.
615 Gadadhar, S., S. Bodakuntla, K. Natarajan, and C. Janke. 2017. The tubulin code at a
616 glance. *J Cell Sci*. 130:1347-1353.
617 Hallak, M.E., J.A. Rodriguez, H.S. Barra, and R. Caputto. 1977. Release of tyrosine from
618 tyrosinated tubulin. Some common factors that affect this process and the assembly
619 of tubulin. *FEBS Lett*. 73:147-150.
620 Hollenbeck, P.J., and W.M. Saxton. 2005. The axonal transport of mitochondria. *J Cell Sci*.
621 118:5411-5419.
622 Janke, C., K. Rogowski, D. Wloga, C. Regnard, A.V. Kajava, J.M. Strub, N. Temurak, J. van
623 Dijk, D. Boucher, A. van Dorsselaer, S. Suryavanshi, J. Gaertig, and B. Eddé. 2005.
624 Tubulin polyglutamylase enzymes are members of the TTL domain protein family.
625 *Science*. 308:1758-1762.
626 Kalfayan, L., and P.C. Wensink. 1982. Developmental regulation of Drosophila alpha-tubulin
627 genes. *Cell*. 29:91-98.
628 Kato, Y., and A. Nakamura. 2012. Roles of cytoplasmic RNP granules in intracellular RNA
629 localization and translational control in the Drosophila oocyte. *Dev Growth Differ*.
630 54:19-31.
631 L'Hernault, S.W., and J.L. Rosenbaum. 1985. Chlamydomonas alpha-tubulin is
632 posttranslationally modified by acetylation on the epsilon-amino group of a lysine.
633 *Biochemistry*. 24:473-478.
634 Lee, G.S., Y. He, E.J. Dougherty, M. Jimenez-Movilla, M. Avella, S. Grullon, D.S. Sharlin, C.
635 Guo, J.A. Blackford, Jr., S. Awasthi, Z. Zhang, S.P. Armstrong, E.C. London, W.
636 Chen, J. Dean, and S.S. Simons, Jr. 2013. Disruption of Ttll5/stamp gene (tubulin
637 tyrosine ligase-like protein 5/SRC-1 and TIF2-associated modulatory protein gene) in
638 male mice causes sperm malformation and infertility. *J Biol Chem*. 288:15167-15180.
639 Lu, W., M. Lakonishok, A.S. Serpinskaya, D. Kirchenbüechler, S.C. Ling, and V.I. Gelfand.
640 2018. Ooplasmic flow cooperates with transport and anchorage in. *J Cell Biol*.
641 217:3497-3511.
642 Lu, W., M. Winding, M. Lakonishok, J. Wildonger, and V.I. Gelfand. 2016. Microtubule-
643 microtubule sliding by kinesin-1 is essential for normal cytoplasmic streaming in
644 Drosophila oocytes. *Proc Natl Acad Sci U S A*. 113:E4995-5004.
645 Magiera, M.M., and C. Janke. 2014. Post-translational modifications of tubulin. *Curr Biol*.
646 24:R351-354.

647 Mahalingan, K.K., E. Keith Keenan, M. Strickland, Y. Li, Y. Liu, H.L. Ball, M.E. Tanner, N.
648 Tjandra, and A. Roll-Mecak. 2020. Structural basis for polyglutamate chain initiation
649 and elongation by TTLL family enzymes. *Nat Struct Mol Biol*. 27:802-813.
650 McKenney, R.J., W. Huynh, R.D. Vale, and M. Sirajuddin. 2016. Tyrosination of α-tubulin
651 controls the initiation of processive dynein-dynactin motility. *Embo j*. 35:1175-1185.
652 Meijering, E., O. Dzyubachyk, and I. Smal. 2012. Methods for cell and particle tracking.
653 *Methods Enzymol*. 504:183-200.
654 Misgeld, T., M. Kerschensteiner, F.M. Bareyre, R.W. Burgess, and J.W. Lichtman. 2007.
655 Imaging axonal transport of mitochondria in vivo. *Nat Methods*. 4:559-561.
656 Pathak, D., K.J. Sepp, and P.J. Hollenbeck. 2010. Evidence that myosin activity opposes
657 microtubule-based axonal transport of mitochondria. *J Neurosci*. 30:8984-8992.
658 Pilling, A.D., D. Horiuchi, C.M. Lively, and W.M. Saxton. 2006. Kinesin-1 and Dynein are the
659 primary motors for fast transport of mitochondria in Drosophila motor axons. *Mol Biol*
660 *Cell*. 17:2057-2068.
661 Port, F., H.M. Chen, T. Lee, and S.L. Bullock. 2014. Optimized CRISPR/Cas tools for
662 efficient germline and somatic genome engineering in Drosophila. *Proc Natl Acad Sci*
663 *U S A*. 111:E2967-2976.
664 Preston, S.F., G.G. Deanin, R.K. Hanson, and M.W. Gordon. 1979. The phylogenetic
665 distribution of tubulin:tyrosine ligase. *J Mol Evol*. 13:233-244.
666 Prota, A.E., M.M. Magiera, M. Kuijpers, K. Bargsten, D. Frey, M. Wieser, R. Jaussi, C.C.
667 Hoogenraad, R.A. Kammerer, C. Janke, and M.O. Steinmetz. 2013. Structural basis
668 of tubulin tyrosination by tubulin tyrosine ligase. *J Cell Biol*. 200:259-270.
669 Redeker, V., N. Levilliers, J.M. Schmitter, J.P. Le Caer, J. Rossier, A. Adoutte, and M.H. Bré.
670 1994. Polyglycylation of tubulin: a posttranslational modification in axonemal
671 microtubules. *Science*. 266:1688-1691.
672 Redeker, V., N. Levilliers, E. Vinolo, J. Rossier, D. Jaillard, D. Burnette, J. Gaertig, and M.H.
673 Bré. 2005. Mutations of tubulin glycylation sites reveal cross-talk between the C
674 termini of alpha- and beta-tubulin and affect the ciliary matrix in Tetrahymena. *J Biol*
675 *Chem*. 280:596-606.
676 Redeker, V., R. Melki, D. Promé, J.P. Le Caer, and J. Rossier. 1992. Structure of tubulin C-
677 terminal domain obtained by subtilisin treatment. The major alpha and beta tubulin
678 isotypes from pig brain are glutamylated. *FEBS Lett*. 313:185-192.
679 Rüdiger, A.H., M. Rüdiger, J. Wehland, and K. Weber. 1999. Monoclonal antibody ID5:
680 epitope characterization and minimal requirements for the recognition of
681 polyglutamylated alpha- and beta-tubulin. *Eur J Cell Biol*. 78:15-20.
682 Schindelin, J., I. Arganda-Carreras, E. Frise, V. Kaynig, M. Longair, T. Pietzsch, S. Preibisch,
683 C. Rueden, S. Saalfeld, B. Schmid, J.Y. Tinevez, D.J. White, V. Hartenstein, K.

684 Eliceiri, P. Tomancak, and A. Cardona. 2012. Fiji: an open-source platform for
685 biological-image analysis. *Nat Methods*. 9:676-682.
686 Sirajuddin, M., L.M. Rice, and R.D. Vale. 2014. Regulation of microtubule motors by tubulin
687 isotypes and post-translational modifications. *Nat Cell Biol*. 16:335-344.
688 St Johnston, D., D. Beuchle, and C. Nüsslein-Volhard. 1991. Staufen, a gene required to
689 localize maternal RNAs in the Drosophila egg. *Cell*. 66:51-63.
690 Stone, M.C., F. Roegiers, and M.M. Rolls. 2008. Microtubules have opposite orientation in
691 axons and dendrites of Drosophila neurons. *Mol Biol Cell*. 19:4122-4129.
692 Suter, B. 2018. RNA localization and transport. *Biochim Biophys Acta Gene Regul Mech*.
693 1861:938-951.
694 Suter, B., and R. Steward. 1991. Requirement for phosphorylation and localization of the
695 Bicaudal-D protein in Drosophila oocyte differentiation. *Cell*. 67:917-926.
696 Theurkauf, W.E., H. Baum, J. Bo, and P.C. Wensink. 1986. Tissue-specific and constitutive
697 alpha-tubulin genes of Drosophila melanogaster code for structurally distinct proteins.
698 *Proc Natl Acad Sci U S A*. 83:8477-8481.
699 Vagnoni, A., and S.L. Bullock. 2016. A simple method for imaging axonal transport in aging
700 neurons using the adult Drosophila wing. *Nat Protoc*. 11:1711-1723.
701 Vallotton, P., and S. Olivier. 2013. Tri-track: free software for large-scale particle tracking.
702 *Microsc Microanal*. 19:451-460.
703 van Dijk, J., K. Rogowski, J. Miro, B. Lacroix, B. Eddé, and C. Janke. 2007. A targeted
704 multienzyme mechanism for selective microtubule polyglutamylation. *Mol Cell*.
705 26:437-448.
706 Wang, X., and T.L. Schwarz. 2009. The mechanism of Ca2+ -dependent regulation of
707 kinesin-mediated mitochondrial motility. *Cell*. 136:163-174.
708 Wang, X., D. Winter, G. Ashrafi, J. Schlehe, Y.L. Wong, D. Selkoe, S. Rice, J. Steen, M.J.
709 LaVoie, and T.L. Schwarz. 2011. PINK1 and Parkin target Miro for phosphorylation
710 and degradation to arrest mitochondrial motility. *Cell*. 147:893-906.
711 Weil, T.T. 2014. mRNA localization in the Drosophila germline. *RNA Biol*. 11:1010-1018.
712 Wloga, D., D.M. Webster, K. Rogowski, M.H. Bré, N. Levilliers, M. Jerka-Dziadosz, C. Janke,
713 S.T. Dougan, and J. Gaertig. 2009. TTLL3 Is a tubulin glycine ligase that regulates
714 the assembly of cilia. *Dev Cell*. 16:867-876.
715 Wolff, A., B. de Néchaud, D. Chillet, H. Mazarguil, E. Desbruyères, S. Audebert, B. Eddé, F.
716 Gros, and P. Denoulet. 1992. Distribution of glutamylated alpha and beta-tubulin in
717 mouse tissues using a specific monoclonal antibody, GT335. *Eur J Cell Biol*. 59:425-
718 432.

719 Zheng, Y., J. Wildonger, B. Ye, Y. Zhang, A. Kita, S.H. Younger, S. Zimmerman, L.Y. Jan,
720 and Y.N. Jan. 2008. Dynein is required for polarized dendritic transport and uniform
721 microtubule orientation in axons. *Nat Cell Biol*. 10:1172-1180.
722 Zimyanin, V.L., K. Belaya, J. Pecreaux, M.J. Gilchrist, A. Clark, I. Davis, and D. St Johnston.
723 2008. In vivo imaging of oskar mRNA transport reveals the mechanism of posterior
724 localization. *Cell*. 134:843-853.

725

726 **Table 1 Conservation between mammalian *TTLL5 and Drosophila TTLL5***
727 Residues labeled in red are critical residues for α-tubulin glutamylation by murine TTLL5 and are
728 conserved in human and *Drosophila* TTLL5 (van Dijk et al., 2007).

	K131 β6-7 loop (R188) R225 E366 N368
Mm TTLL5	TRKDR--KPVASSRGRGVY---VRLYVL---LLEVNLSP
Hs TTLL5	TRKDR--KPVASSRGRGVY---VRLYVL---LLEVNLSP
	K282 β6-7 loop (R339) R376 E517 N519
Dm TTLL5	TRKDR--KPAASSRGRG I F---LRVYVL---LLEI NLSP

729

730

731 **Table 2 Conservation between *TTL* and *TTLL5***
732 Many critical residues of human TTL (red) are conserved in *Drosophila,* mouse and human TTLL5 (Prota et al.,
733 2013; van Dijk et al., 2007).

	R202 R222 D318 E331 N333 P336
Hs TTL	IRSW--VLRTA-----FDFM--LI EVNGAPA
	R376 R398 D504 E517 N519 P522
Dm TTLL5	LRVY---I VRLA-----FDIL----LLEI NL SPS
	R225 R247 D353 E366 N368 P371
Mm TTLL5	VRLY---LARFA-----FDVL---LLEVNL SPS
Hs TTLL5	VRLY---LARFA-----FDVL---LLEVNL SPS

734

735

736 **Table 3 Transport parameters for mitochondria in the selected region of L1 veins.**

Genotype	*Control*		*TTLL5^{E517A}*	
Direction	Plus-end	Minus-end	Plus-end	Minus-end
Number of wings (motile mito[1)])	3 (20)	3 (11)	3 (8)	3 (2)
Motile Mito[1)] (% total mito)	5.3±1.7	2.5±3.2	**1.5±1.3***	0.4±0.4
Total time (s)	92±45	100±43	98±48	64±37
Pausing (% total time)[2)]	74±14	77±15	**63±13***	61±20
Length (μm)	7.2±4.5	6.7±1.6	**12.3±5.3***	7.5±2.8
Velocity (μm/s)[3)]	0.37±0.08	0.38±0.14	0.36±0.08	0.36±0.16

737 [1)] Motile mitochondria showed a run distance ≥ 2 μm.
738 [2)] The pausing time ratio indicates the pausing time divided by the total duration of each motile mitochondria.
739 [3)] Mean velocity corresponds to the mean values of instant trafficking velocity. Significant differences for
740 mitochondria of plus-end transport between control and *TTLL5^{E517A}* is shown in bold face followed by * ($p<0.05$).
741 Only two mitochondria transported toward the MT minus-end were observed in *TTLL5^{E517A}*. A comparison of the

742 minus-end transport between control and *TTLL5*^{E517A} is not warranted, and these parts are shaded in grey to
743 indicate this.

744

745 **Figure legends**

746

747 **Fig. 1 Schematic representation of the *Drosophila TTLL5* gene, TTLL5, TTLL5^{MiEx}, and**
748 **Venus::TTLL5 protein.** A) The *TTLL5* gene structure is based on the Flybase data for the
749 CG31108-RA transcript. The positions of the loss-of-function mutations are marked on the
750 *TTLL5* gene. Grey triangles: transposon insertions. Grey asterisks: codons targeted for
751 generating InDels and point mutations. All *TTLL5* alleles were analyzed as hemizygous
752 animals over *Df(3R)BSC679*, which removes the region of the *TTLL5* gene. B) Western blot
753 from the soluble fraction of ovarian extracts. *w* (*TTLL5*$^{+}$/$^{+}$*),* which contains 2 wild-type copies
754 of *TTLL5*, expressed the highest levels of TTLL5. The TTLL5 signal is strongly reduced or
755 abolished in the null mutants *TTLL5*^{pBac}/-*, TTLL5*^{Mi}/- and *TTLL5*^{MiEx}/- compared to *w.* The
756 hemizygous *TTLL5*$^{+}$ ovaries (*TTLL5*$^{+}$/-) expressed less TTLL5 than *w.* The signal of an
757 unspecific band (labeled with *), produced after a short exposure, was used as loading
758 control. In the following we will refer to the genotypes as *w* for the control (*TTLL5*$^{+}$/$^{+}$) and as
759 *TTLL5*^{allele} for the hemizygous mutants *(TTLL5*^{allele}/ $^{-}$).

760

761 **Fig. 2 Mass spectrometry analysis of the glutamylation of the C-terminal domains of**
762 **the α-tubulin isoforms.** A) In *Drosophila* ovaries**,** the C-terminal peptides of TBA1/3 can be
763 found modified by glutamic acids residue added to the side chains of E443, E445, E448, and
764 E449**.** B) The C-terminal peptides containing the full primary sequence were analyzed. The
765 structure of the different C-terminal tail peptides of TBA1/3 modified by glutamylation are
766 shown. Different combinations of Glu side chain modifications were found added at the
767 positions E443, E445, E448, and E449 of TBA1/3. C) Frequency of glutamylated C-terminal
768 peptides (containing the entire primary sequence) in *w* controls, *TTLL5*^{pBac} and *TTLL5*^{MiEx}
769 mutants containing modifications of 1E, 2E or 3Es. “Total Glu modification” shows the sum of
770 the 3 frequencies. The ratio was quantified based on the values of glutamylated C-terminal
771 TBA1/3 PSM (peptide spectrum match) divided by total PSM of the full primary C-terminal
772 TBA1/3 sequence.

773

774 **Fig. 3 *TTLL5* is required for the glutamylation of the TBA1/3 isoforms of ovarian α-**
775 **tubulin.** A) A’) Sites on TBA1/3 recognized by the GT335 and 1D5 antibodies, respectively.
776 B) B’) B’’) The glutamylation signal produced by western blotting with the GT335 and 1D5

777 antibodies is lower in *TTLL5*^{pBac}*, TTLL5*^{Mi}, and *TTLL5*^{MiEx} than in the *w* control, but is restored
778 and even elevated in mutant ovaries that were rescued by *MattubGal4>Venus::TTLL5*. The
779 up-shifted bands recognized by 1D5 can be seen in the rescued *TTLL5*^{pBac} and *TTLL5*^{Mi}
780 mutants. The total tyrosinated α-tubulin levels seemed unaffected by the TTLL5 levels. B'')
781 The anti-βmono-E levels were similar between *w* control, *TTLL5*^{MiEx}, and rescue of *TTLL5*^{MiEx}.
782 α-tubulin and GAPDH served as loading controls. C) Stronger up-shifted bands were
783 observed upon *MattubGal4>Venus::TTLL5* overexpression in wild-type ovaries (anti-1D5
784 antibody). Total α-tubulin remained at similar levels in samples with excessive expression of
785 *TTLL5.* GAPDH was a loading control. D) The genotypes and rational of the *TTLL5* alleles
786 generated by Crispr/Cas9 are listed. The selected residues are predicted to be either
787 important for the glutamylation or tyrosination function based on the alignment shown in
788 **Tables 1** and **2**. E) Western blotting showed that the polyglutamylation signal is absent in all
789 point mutants. *w* with 2 copies of *TTLL5*$^{+}$ is the wild-type control and *TTLL5*^{K282} indel
790 (*TTLL5*$^{K282\ indel3}$) that with only one copy of *TTLL5* still kept K282 is therefore an additional
791 control. Relative 1D5 level was observed slightly decreased in the hemizygous situation with
792 only one *TTLL5* copy. All *TTLL5* alleles were analyzed as hemizygous animals over
793 *Df(3R)BSC679*, which removes the region of the *TTLL5* gene. The genotypes for rescues
794 were *MattubGal4>UAS-Venus::TTLL5;TTLL5*^{alleles}*/Df(3R)BSC679.* The genotypes for
795 *Venus::TTLL5* overexpression were *MattubGal4>UAS-Venus::TTLL5 ;*

796

797 **Fig. 4 Effect of *TTLL5* on Staufen posterior localization refinement in oocytes.**
798 A) A') Confocal micrographs showing stage 10B oocytes of *w* controls and *TTLL5*^{pBac}*,*
799 *TTLL5*^{Mi}, and *TTLL5*^{MiEx} mutants. A'') Confocal micrographs showing stage 10B oocytes of
800 *TTLL5*^{pBac}*, TTLL5*^{Mi}, and *TTLL5*^{MiEx} mutants and their rescue with *Mattub4>UASP-*
801 *Venus::TTLL5*. Anti-Staufen is shown in green, anti-GFP in red, and Hochest in blue. A''')
802 Quantification of the Staufen crescent length along the posterior cortex based on A, A' and
803 A''. B) B') Confocal micrographs showing stage 10B oocytes of *w* controls, *TTLL5*^{E517A}*,*
804 *TTLL5*^{P522A}*,* and *TTLL5*^{R339A} mutants. B'') Quantification of Staufen's crescent length along
805 the posterior cortex based on B and B'', respectively. C) C') Confocal micrographs showing
806 previtellogenic egg chambers of *w* controls, *TTLL5*^{E517A}*, TTLL5*^{P522A}*,* and *TTLL5*^{R339A} mutants.
807 anti-BicD is shown in red, anti-Staufen in green, and Hochest in blue. D) The BicD levels
808 remained unchanged between *w* control, *TTLL5*^{MiEx}, and *TTLL5*^{MiEx} rescued by
809 *Mattub4>Venus::TTLL5.* GAPDH served as loading control. *** $p<0.005$; ** <0.01. Scale Bar:
810 25 μm. All *TTLL5* alleles were hemizygous over *Df(3R)BSC679*. The genotypes for rescued
811 animals were *MattubGal4/UAS-Venus::TTLL5;TTLL5* ^{alleles}*/Df(3R)BSC679.*

812

813 **Fig. 5 Role of *TTLL5* in ooplasmic streaming.** A) KHC levels remained unchanged
814 between *w* control, *TTLL5*^{MiEx}, and *TTLL5*^{MiEx} rescued by *Mattub4>Venus::TTLL5.* GAPDH
815 served as loading control. B) Example picture of a stage 10B oocyte used for particle flow
816 measurements based on time-lapse movies of ooplasmic streaming (Mov.S1-S4). Scale Bar:
817 25 µm. C) 100-200 particles were selected along the cortex line from two sides of each
818 ooplasm to determine the mean velocities of the particles from the different genotypes. One
819 stage 10B oocyte was chosen randomly for velocity quantification for each fly. The fly
820 numbers for *w* control, *TTLL5*^{MiEx} mutant, *TTLL5*^{E517A} mutant, and *UASP-Venus::TTLL5*
821 transgene rescuing the *TTLL5*^{MiEx} mutant were 7, 9, 5, and 5, respectively. No significant
822 changes of particle velocity were found between different genotypes. D) Representative
823 kymographs of particles in oocytes of a *w* control, a *TTLL5*^{MiEx} mutant, the *TTLL5*^{E517A} mutant
824 and the *TTLL5*^{MiEx} mutant rescued by overexpression of the *UASP-Venus::TTLL5* transgene.
825 Kymographs were generated along a line (the yellow line in B) close to the cortex on each
826 side of the ooplasm from 3 min time-lapse movies. Representative kymographs showed that
827 the lines generated along the cortex were parallel to the particle flow in both control and
828 *Venus::TTLL5* rescue. The moving particles revealed different flow patterns in the case
829 when TTLL5 activity was low. Genotypes for *TTLL5*^{MiEx} and *TTLL5*^{E517A} were
830 *TTLL5*^{MiEx}*/Df(3R)BSC679* and *TTLL5*^{E517A}*/Df(3R)BSC679*, respectively. The genotype of the
831 rescued flies was *MattubGal4/UAS-Venus::TTLL5; TTLL5*^{MiEx}*/Df(3R)BSC679.*

832

833 **Fig. 6 Effect of *TTLL5* on mitochondria transport in the wing nerve.** A) In head and wing
834 extracts, the relative glutamylation signal of 1D5 is lower in *TTLL5*^{E517A} (genotype: *ApplGal4;*
835 *UAS-Mito::GFP; TTLL5*^{E517A}*/Df(3R)BSC679*) than in the control (genotype: *ApplGal4;UAS-*
836 *Mito::GFP;+/Df(3R)BSC679*). B) Cartoon of the *Drosophila* wing showing the L1 and L3 vein
837 and the neuron rich regions analyzed for tracking mitochondria (red and green boxes). C)
838 Representative still image of GFP-labelled mitochondria in axons of the L1 and L3 vein (from
839 **Mov. S5** and **Mov. S6**, respectively) of both control and *TTLL5*^{E517A} wings. Transported
840 mitochondria (run distance ≥ 2 µm) were manually labeled with the Fiji MTrackJ plugin.
841 Some circles only mark a mitochondrial signal that appeared in another time frame. Scale
842 Bar: 10 µm. D) Quantification of the fraction of transported mitochondria. Note that in control
843 wings a much higher fraction of mitochondria is transported in the L3 vein than in L1. The
844 results from L1 show a dramatic decrease of motile mitochondria in the *TTLL5*^{E517A} mutant.
845 In the L3 vein, no transported mitochondria were found in the *TTLL5*^{E517A} mutant. The total

846 particles (indicated by “n”) with the diameter from 0.1μm-1.6μm were analyzed by Fiji from
847 the signals of representative still images from three wings for each genotype. The motile
848 mitochondria ratio indicates the value of transported mitochondria divided by total
849 mitochondria particles. E) Scheme of the transport behavior of the mitochondria in the wing
850 neuron. Start of a run was either considered the time when a motile particle began to move
851 from a stationary position or entered into the focal plane. Particles were defined as
852 “trafficking” when their instant velocity was ≥ 0.2 μm/s and they were considered as “pausing”
853 when they moved at less than 0.2 μm/s, but later resumed their movement. As stop of a run
854 we considered particles that entirely terminated or moved out of the focal plane. For each
855 run, the total run distance of more than 2 μm was considered as “transported or motile
856 mitochondria”. *** $p<0.005$; * <0.05.

Fig. 1

A

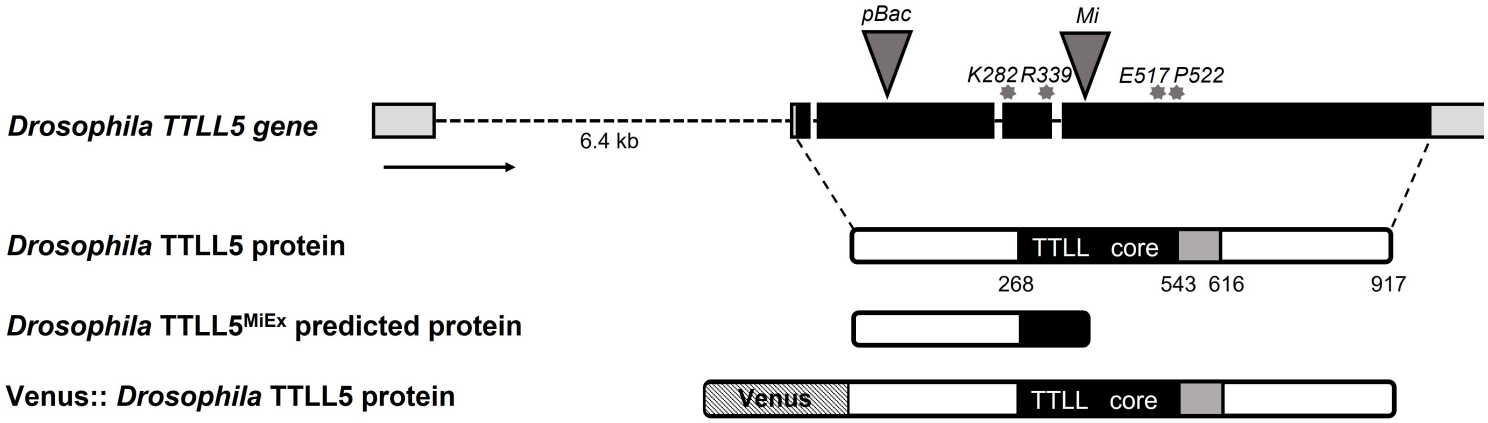
pBac
Mi
K282 R339
E517 P522
Drosophila TTLL5 gene
6.4 kb
Drosophila TTLL5 protein
TTLL core
268
543 616
917
Drosophila TTLL5MiEx predicted protein
Venus:: Drosophila TTLL5 protein
Venus
TTLL core

B

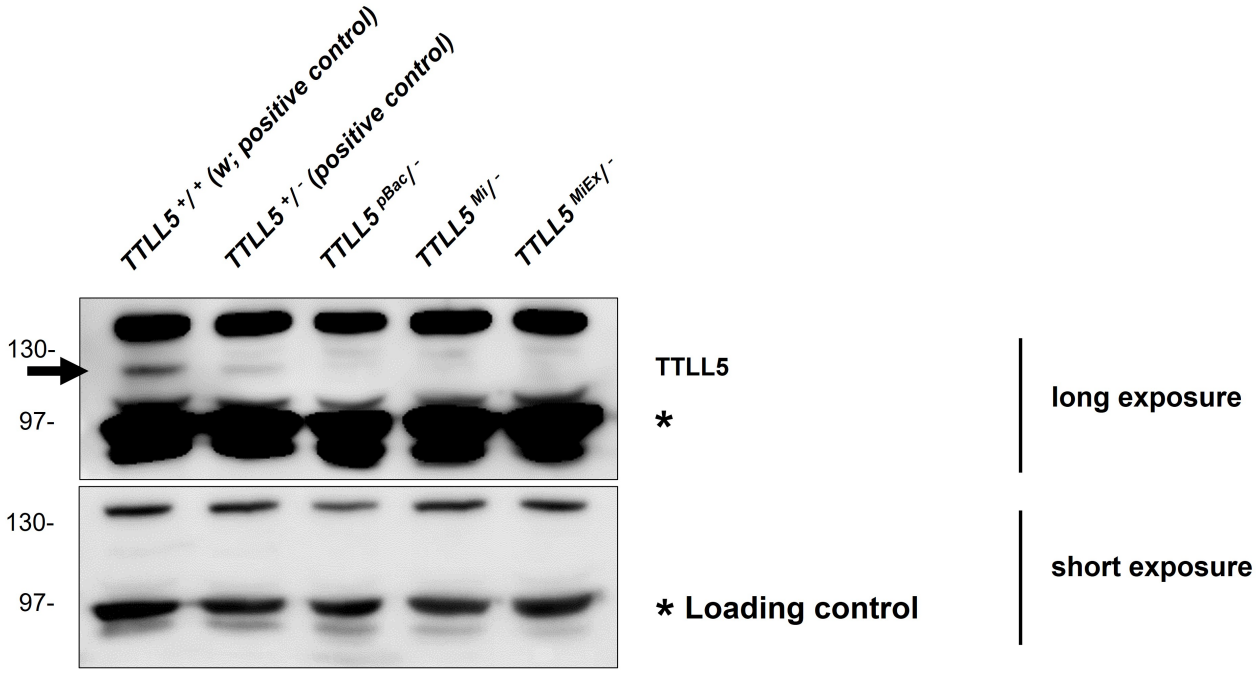
TTLL5 +/+ (w; positive control)
TTLL5 +/- (positive control)
TTLL5 pBac/-
TTLL5 Mi/-
TTLL5 MiEx/-
130-
97-
TTLL5
*
long exposure
130-
97-
* Loading control
short exposure

Fig. 2

A

α-tubulin isoforms in *Drosophila* ovaries

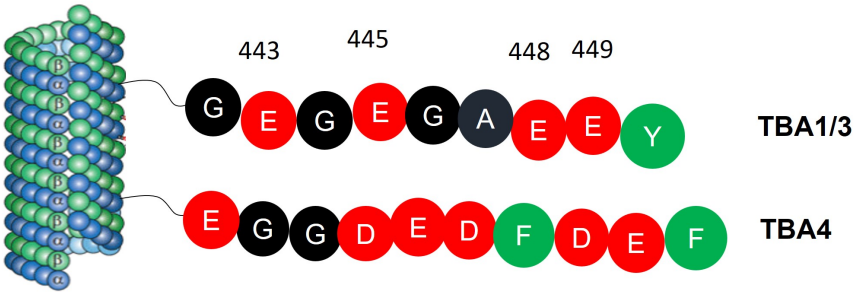

E-residues were found added at the TBA1/3 positions: E443, E445, E448 and E449.

B

Glutamylation on Glu residues in the C-terminal domain of TBA1/3

```
GEGEGAEEY   GEGEGAEEY   GEGEGAEEY   GEGEGAEEY
 |            |            |            |
 E            E            E            E

GEGEGAEEY   GEGEGAEEY   GEGEGAEEY   GEGEGAEEY
 |            |            |            |
 EE           EE           EE           EE

GEGEGAEEY   GEGEGAEEY   GEGEGAEEY   GEGEGAEEY
 |            |            |            |
 EEE          EEE          EEE          EEE

GEGEGAEEY   GEGEGAEEY   GEGEGAEEY   GEGEGAEEY
 |  |         |  |         |    |      |
 E  E         E  EE        E    E      E    EE

GEGEGAEEY   GEGEGAEEY
       | |    |  |    |
       EEE    E  E    E
```

C

Role of *TTLL5* for the Glutamylation of the C-terminal domain of TBA1/3

	w (n=56)	***TTLL5*** ^{pBac} (n=29) (*%E mod*)	***TTLL5*** ^{MiEx} (n=7)
+1	41	0	0
+2	14	0	0
+3	7	0	0
Total Glu modification	**62**	**0**	**0**

Fig. 3

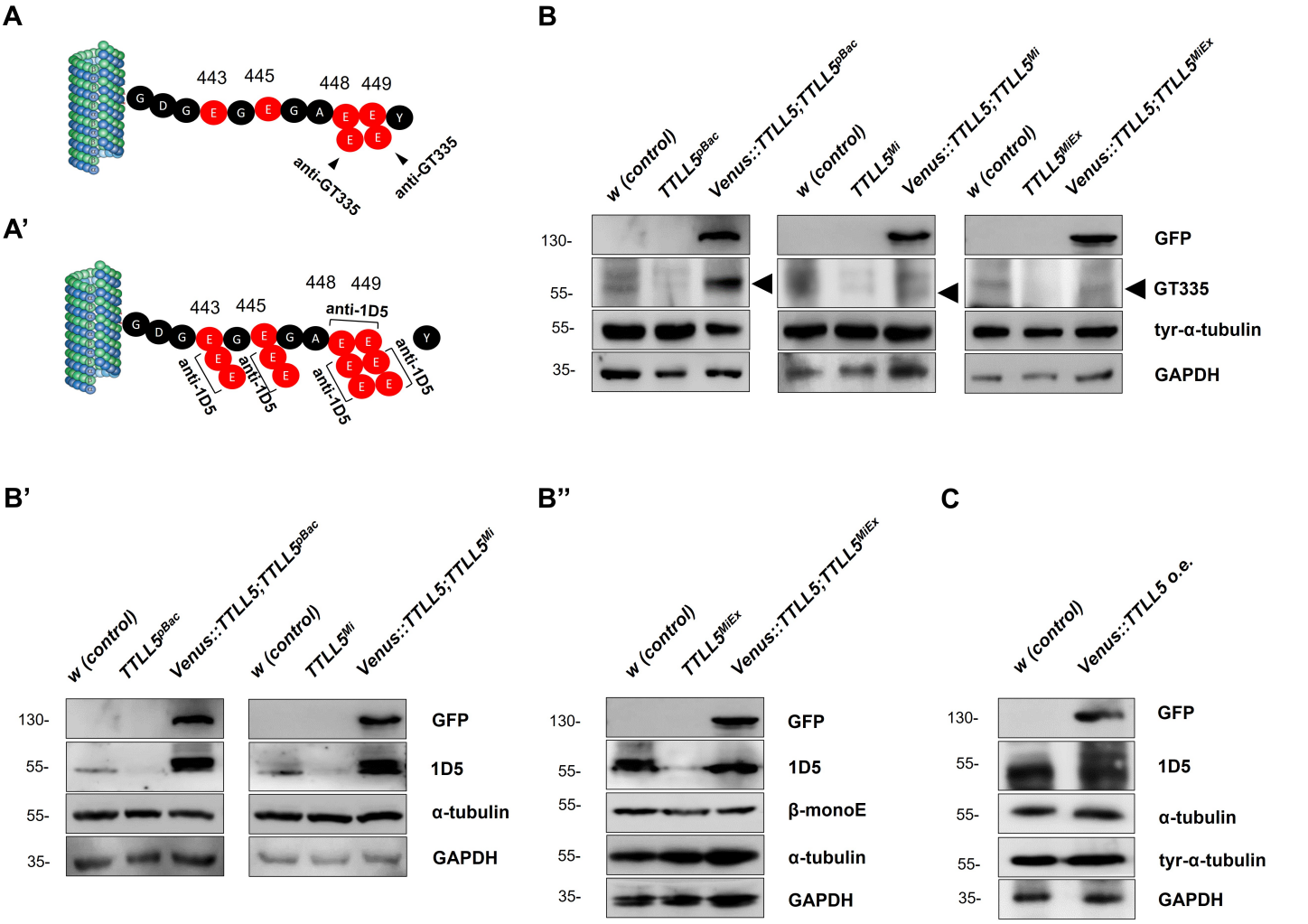

D

Residues of *Drosophila TTLL5*	Function	Corresponding residues to mammalian *TTLL5* or *TTL*	Mutations
E517	ATP/ADP binding	*MmE336 of TTLL5* *HsE331 of TTL*	*E517 indel* : WLLE517 → S E517A
K282	ATP/ADP binding	*MmK131 of TTLL5*	*K282 indel 1* : K282 → stop codon *K282 indel 2* : TRKD283 → N *K282 indel 3* : TRK282 → KGK282
R339	(In β6-7 loop) Stabilization tubulin with TTLL5 active site	*MmR188 of TTLL5*	R339A
P522	(Conserved residue of human TTL) Anchor enzyme to α-tubulin	*HsP336* of *TTL*	P522A

E

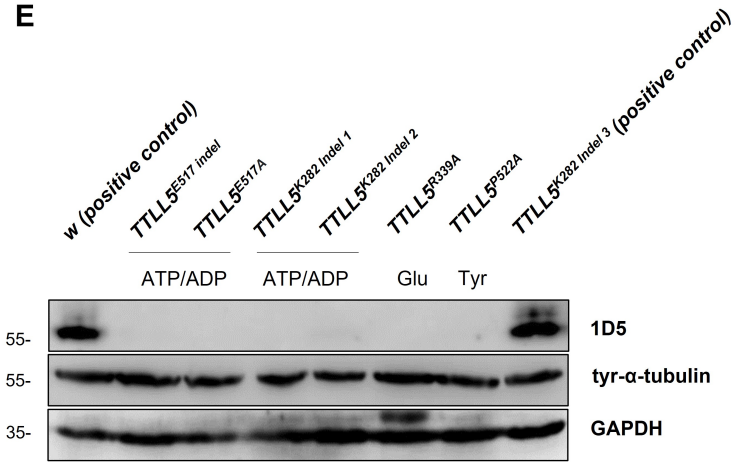

Fig. 4

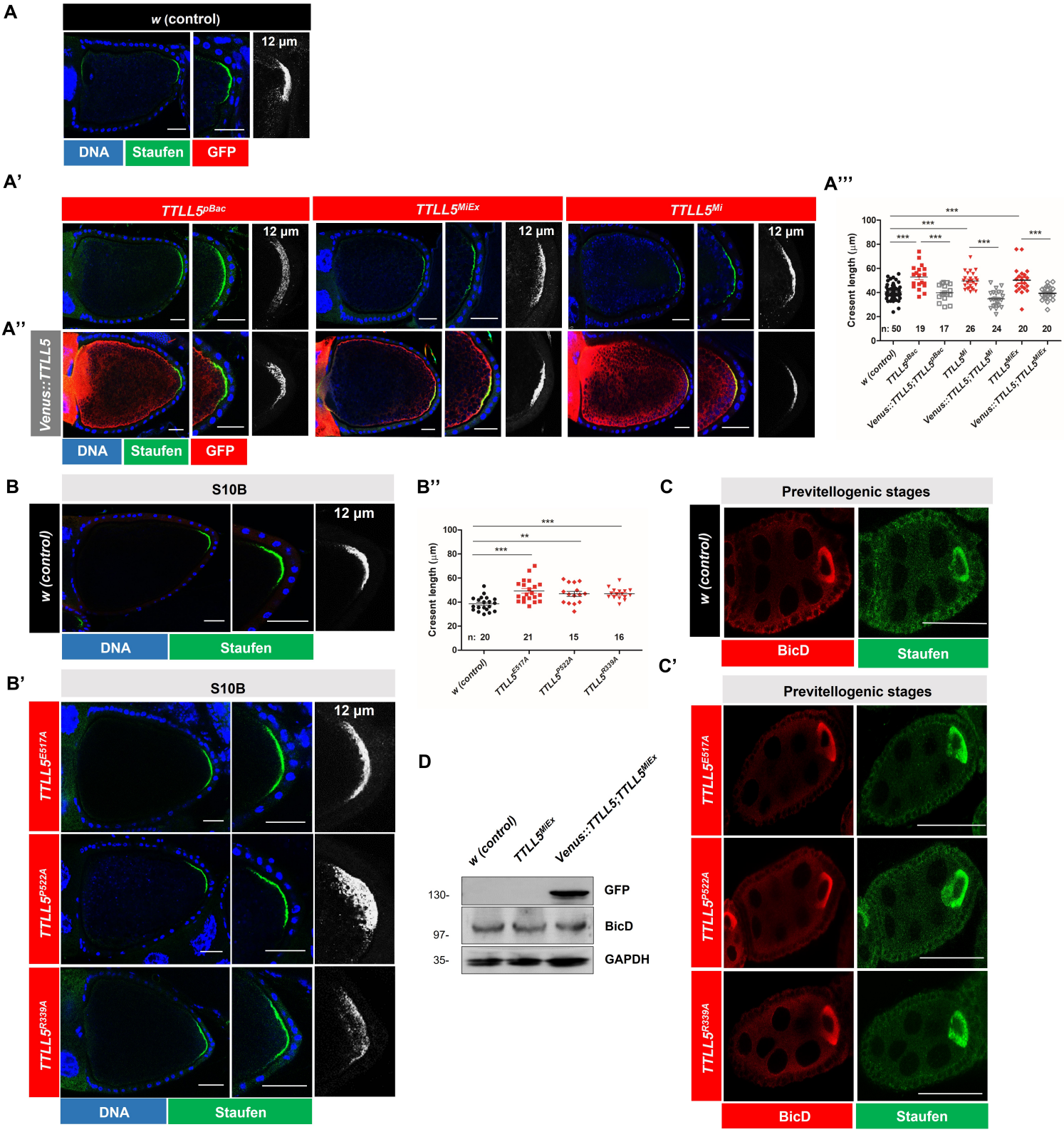
A
w (control)
12 µm
DNA
Staufen
GFP
A'
TTLL5pBac
TTLL5MiEx
TTLL5Mi
12 µm
A''
Venus::TTLL5
DNA
Staufen
GFP
A'''
Cresent length (µm)
n: 50
19
17
26
24
20
20
w (control)
TTLL5pBac
Venus::TTLL5;TTLL5pBac
TTLL5Mi
Venus::TTLL5;TTLL5Mi
TTLL5MiEx
Venus::TTLL5;TTLL5MiEx
B
S10B
w (control)
12 µm
DNA
Staufen
B'
S10B
TTLL5E517A
TTLL5P522A
TTLL5R339A
12 µm
DNA
Staufen
B''
Cresent length (µm)
n: 20
21
15
16
w (control)
TTLL5E517A
TTLL5P522A
TTLL5R339A
C
Previtellogenic stages
w (control)
BicD
Staufen
C'
Previtellogenic stages
TTLL5E517A
TTLL5P522A
TTLL5R339A
BicD
Staufen
D
w (control)
TTLL5MiEx
Venus::TTLL5;TTLL5MiEx
130-
97-
35-
GFP
BicD
GAPDH

Fig. 5

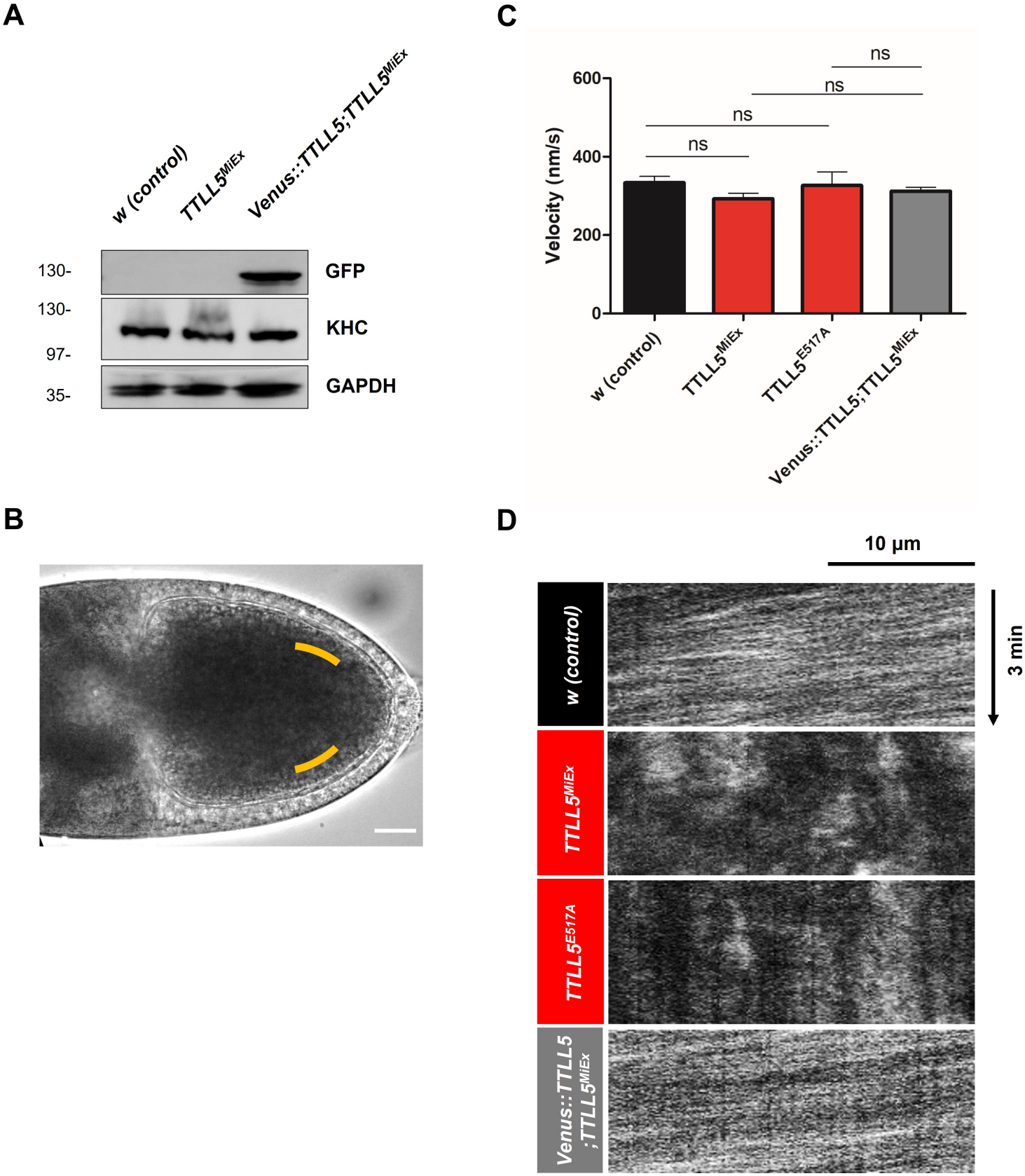
A
w (control)
TTLL5MiEx
Venus::TTLL5;TTLL5MiEx
130-
130-
97-
35-
GFP
KHC
GAPDH
C
Velocity (nm/s)
600
400
200
0
ns
ns
ns
ns
w (control)
TTLL5MiEx
TTLL5E517A
Venus::TTLL5;TTLL5MiEx
B
D
10 µm
3 min
w (control)
TTLL5MiEx
TTLL5E517A
Venus::TTLL5
;TTLL5MiEx

Fig. 6

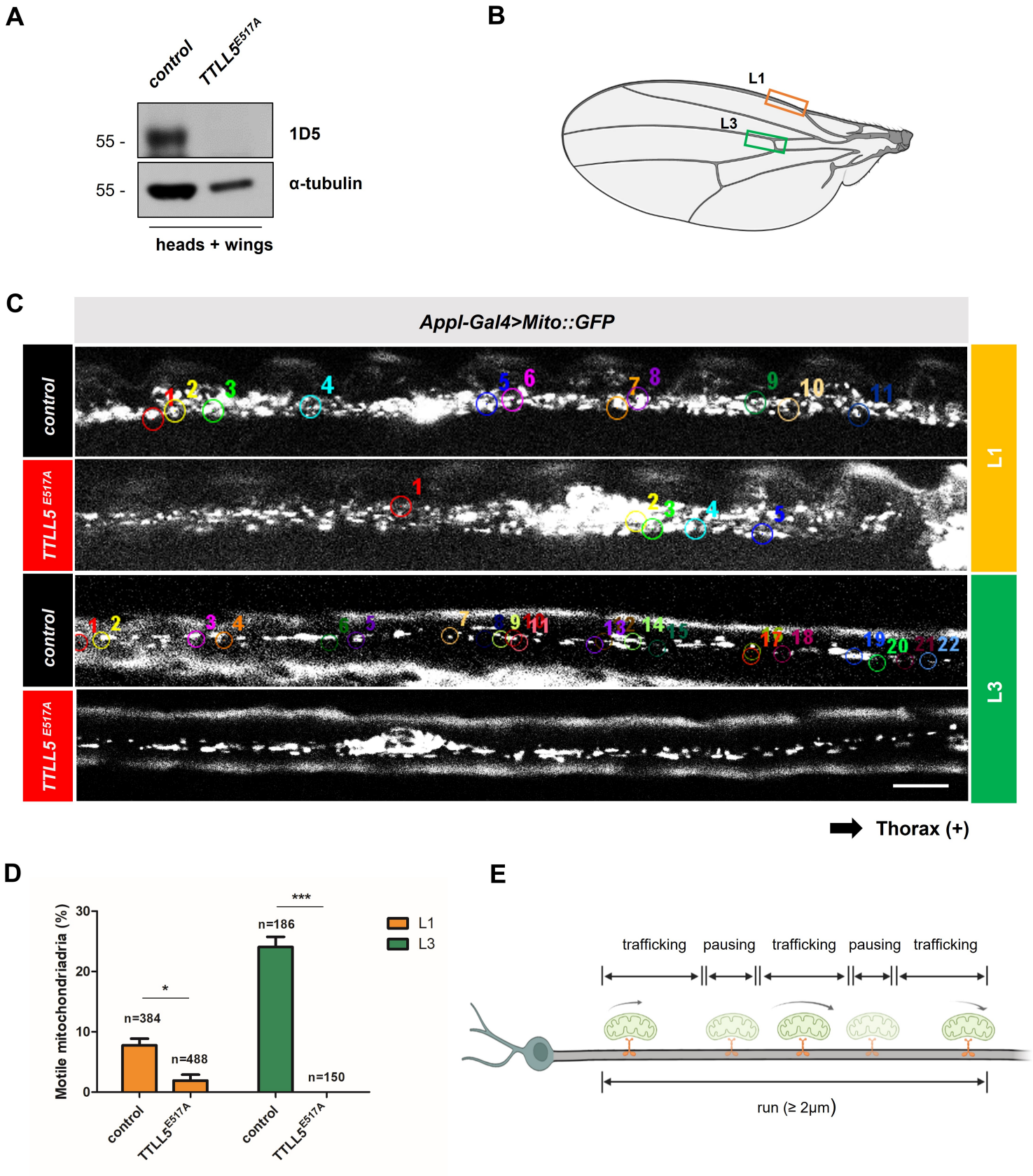
A
control
TTLL5E517A
55 -
55 -
1D5
α-tubulin
heads + wings
B
L1
L3
C
Appl-Gal4>Mito::GFP
control
TTLL5 E517A
control
TTLL5 E517A
L1
L3
Thorax (+)
D
Motile mitochondriadria (%)
30
20
10
0
*
***
n=384
n=488
n=186
n=150
L1
L3
control
TTLL5E517A
control
TTLL5E517A
E
trafficking
pausing
trafficking
pausing
trafficking
run (≥ 2μm)

Fig. S1

A) Example_Es on *w* TBA1/3: GEGEGAEEY
EE

PEAKS

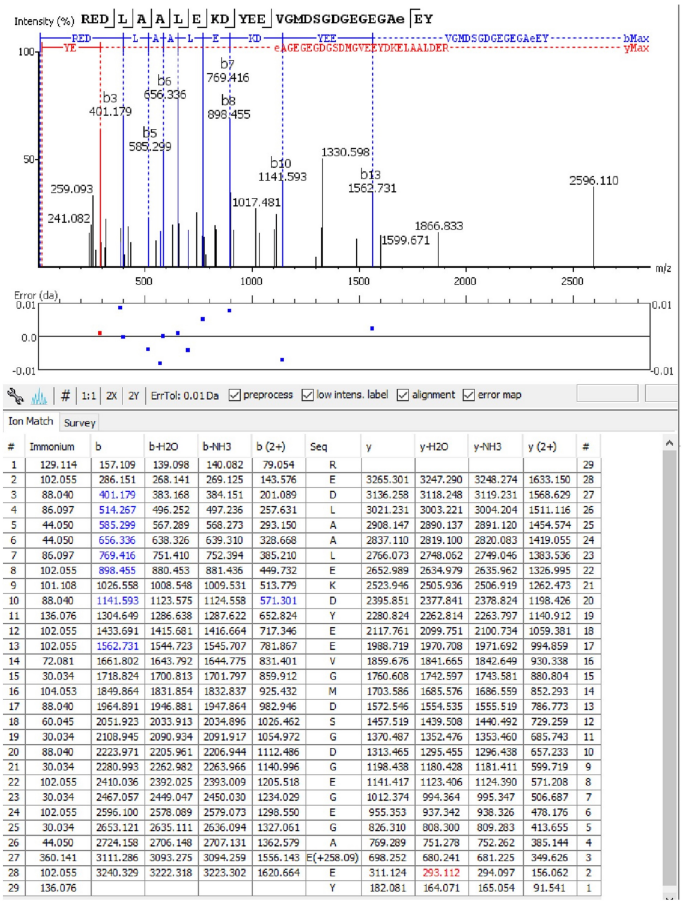

#	Immonium	b	b-H2O	b-NH3	b (2+)	Seq	y	y-H2O	y-NH3	y (2+)	#
1	129.114	157.109	139.098	140.082	79.054	R					29
2	102.055	286.151	268.141	269.125	143.576	E	3265.301	3247.290	3248.274	1633.150	28
3	88.040	401.179	383.168	384.151	201.089	D	3136.258	3118.248	3119.231	1568.629	27
4	86.097	514.257	496.252	497.236	257.631	L	3021.231	3003.221	3004.204	1511.116	26
5	44.050	585.299	567.289	568.273	293.150	A	2908.147	2890.137	2891.120	1454.574	25
6	44.050	656.336	638.326	639.310	328.668	A	2837.110	2819.100	2820.083	1419.055	24
7	86.097	769.416	751.410	752.394	385.210	L	2766.073	2748.062	2749.046	1383.536	23
8	102.055	898.455	880.453	881.436	449.732	E	2652.989	2634.979	2635.962	1326.995	22
9	101.108	1026.558	1008.548	1009.531	513.779	K	2523.946	2505.936	2506.919	1262.473	21
10	88.040	1141.593	1123.575	1124.558	571.301	D	2395.851	2377.841	2378.824	1198.426	20
11	136.076	1304.649	1286.638	1287.622	652.824	Y	2280.824	2262.814	2263.797	1140.912	19
12	102.055	1433.691	1415.681	1416.664	717.346	E	2117.761	2099.751	2100.734	1059.381	18
13	102.055	1562.731	1544.723	1545.707	781.867	E	1988.719	1970.708	1971.692	994.859	17
14	72.081	1661.802	1643.792	1644.775	831.401	V	1859.676	1841.665	1842.649	930.338	16
15	30.034	1718.824	1700.813	1701.797	859.912	G	1760.608	1742.597	1743.581	880.804	15
16	104.053	1849.864	1831.854	1832.837	925.432	M	1703.586	1685.576	1686.559	852.293	14
17	88.040	1964.891	1946.881	1947.864	982.946	D	1572.546	1554.535	1555.519	786.773	13
18	60.045	2051.923	2033.913	2034.896	1026.462	S	1457.519	1439.508	1440.492	729.259	12
19	30.034	2108.945	2090.934	2091.917	1054.972	G	1370.487	1352.476	1353.460	685.743	11
20	88.040	2223.971	2205.961	2206.944	1112.486	D	1313.465	1295.455	1296.438	657.233	10
21	30.034	2280.993	2262.982	2263.966	1140.996	G	1198.438	1180.428	1181.411	599.719	9
22	102.055	2410.036	2392.025	2393.009	1205.518	E	1141.417	1123.406	1124.390	571.208	8
23	30.034	2467.057	2449.047	2450.030	1234.029	G	1012.374	994.364	995.347	506.687	7
24	102.055	2596.100	2578.089	2579.073	1298.550	E	955.353	937.342	938.326	478.176	6
25	30.034	2653.121	2635.111	2636.094	1327.061	G	826.310	808.300	809.283	413.655	5
26	44.050	2724.158	2706.148	2707.131	1362.579	A	769.289	751.278	752.262	385.144	4
27	360.141	3111.286	3093.275	3094.259	1556.143	E(+258.09)	698.252	680.241	681.225	349.626	3
28	102.055	3240.329	3222.318	3223.302	1620.664	E	311.124	293.112	294.097	156.062	2
29	136.076					Y	182.081	164.071	165.054	91.541	1

Easyprot

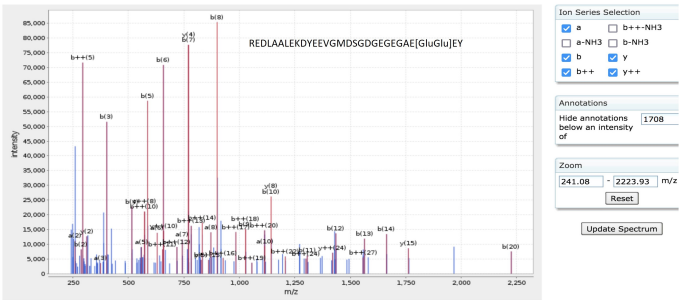

Table of identified ion fragments

Data to display: Fragment Mass (m/z) Peak Intensity: 0-10% 11-30% 31-50% 51-70% 71-100%

13	14	15	16	17	18	19	20	21	22	23	24	25	26	27	28	29
2.725	1661.82						2223.926									
.6734	831.4086	859.9195	925.4355	982.9461	1026.50	1054.986	1112.48		1205.521		1298.564			1556.151		
				974.4438			1103.981									
E	V	G	M	D	S	G	D	G	E	G	E	G	A	E	E	Y
		1760.615							1141.584			826.296	769.4193		311.124	
							657.3403		571.2989							
17	16	15	14	13	12	11	10	9	8	7	6	5	4	3	2	1

B) Example_*w* TBA4: DEDFDEF

MSfragger

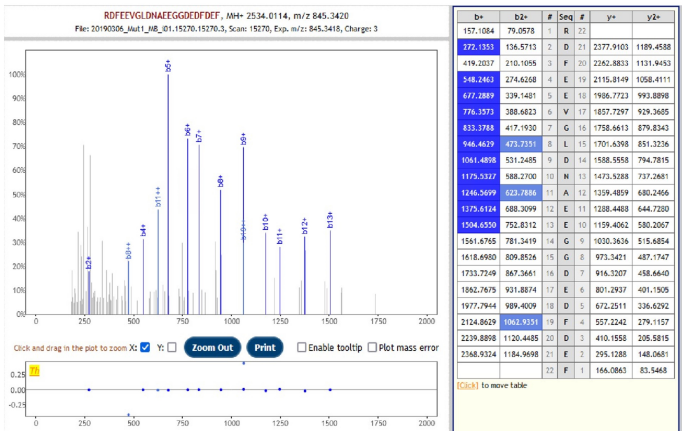

b+	b2+	#	Seq	#	y+	y2+
157.1084	79.0578	1	R	22		
272.1353	136.5713	2	D	21	2377.9103	1189.4588
419.2037	210.1055	3	F	20	2262.8833	1131.9453
548.2463	274.6268	4	E	19	2115.8149	1058.4111
677.2889	339.1481	5	E	18	1986.7723	993.8898
776.3573	388.6823	6	V	17	1857.7297	929.3685
833.3788	417.1930	7	G	16	1758.6613	879.8343
946.4629	473.7351	8	L	15	1701.6398	851.3236
1061.4898	531.2485	9	D	14	1588.5558	794.7815
1175.5327	588.2700	10	N	13	1473.5288	737.2681
1246.5699	623.7886	11	A	12	1359.4859	680.2466
1375.6124	688.3099	12	E	11	1288.4488	644.7280
1504.6550	752.8312	13	E	10	1159.4062	580.2067
1561.6765	781.3419	14	G	9	1030.3636	515.6854
1618.6980	809.8526	15	G	8	973.3421	487.1747
1733.7249	867.3661	16	D	7	916.3207	458.6640
1862.7675	931.8874	17	E	6	801.2937	401.1505
1977.7944	989.4009	18	D	5	672.2511	336.6292
2124.8629	1062.9351	19	F	4	557.2242	279.1157
2239.8898	1120.4485	20	D	3	410.1558	205.5815
2368.9324	1184.9698	21	E	2	295.1288	148.0681
		22	F	1	166.0863	83.5468

[Click] to move table

Fig. S2

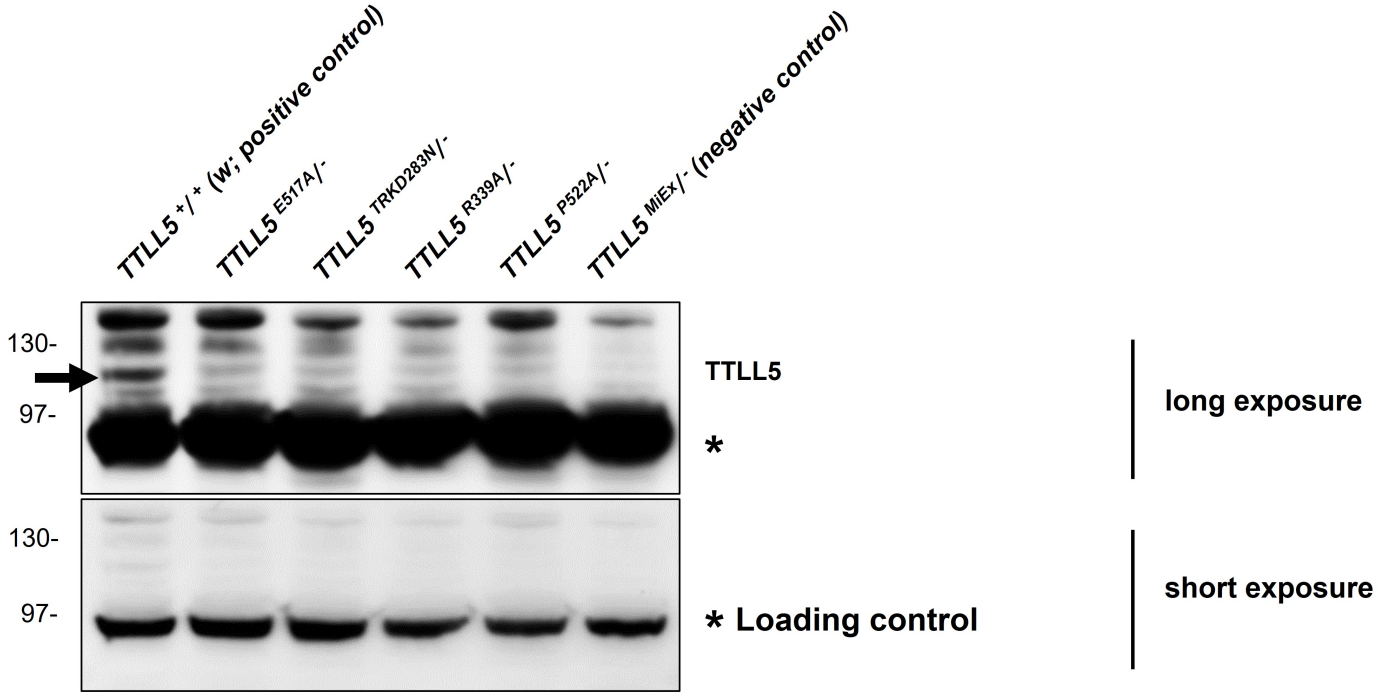
TTLL5 */+ (w; positive control)
TTLL5 E517A/-
TTLL5 TRKD283N/-
TTLL5 R339A/-
TTLL5 P522A/-
TTLL5 MiEx/- (negative control)
130-
97-
TTLL5
*
long exposure
130-
97-
* Loading control
short exposure

Fig. S3

A

α-tubulin isoforms in *Drosophila* ovaries

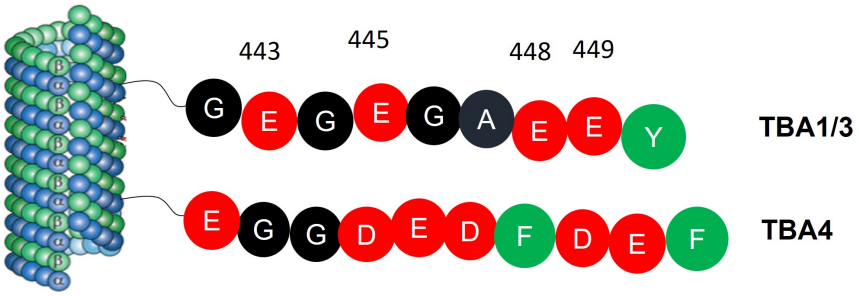

G-residues were found added at the TBA1/3 positions E443, E445, E448 and E449.

B

Glycylation on Glu residues in the C-terminal domain of TBA1/3

GEGEGAEEY G	GEGEGAEEY G	GEGEGAEEY G	GEGEGAEEY G G
GEGEGAEEY GG	GEGEGAEEY GG	GEGEGAEEY GG	GEGEGAEEY GG

C

Role of *TTLL5* for the Glycylation of the C-terminal domain of TBA1/3

	w (n=56)	***TTLL5*** ^{pBac} (n=29) (*%G mod*)	***TTLL5*** ^{MiEx} (n=7)
+1	3.5	10	14
+2	3.5	0	0
Total Gly modification	**7**	**10**	**14**

Fig. S4

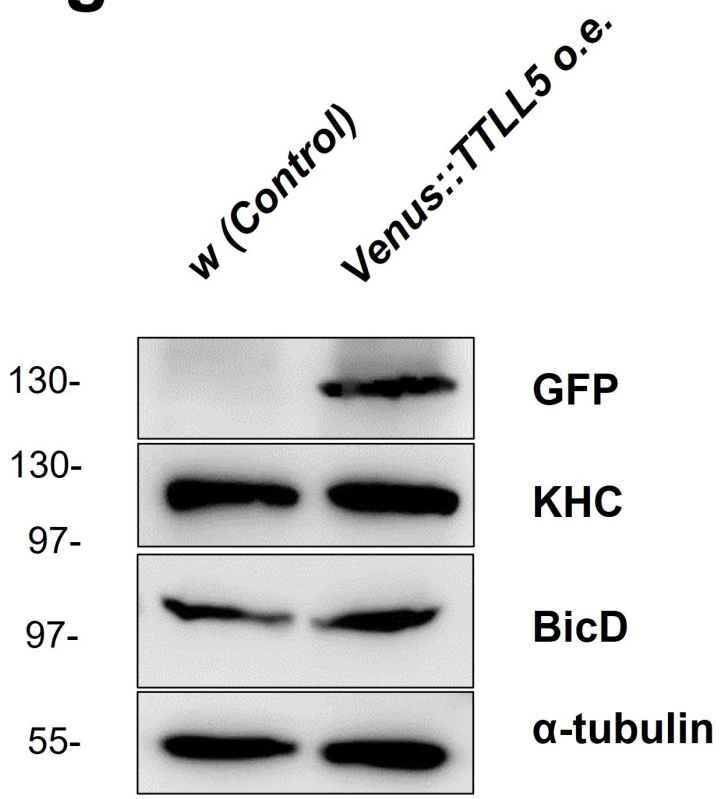
w (Control)
Venus::TTLL5 o.e.
130-
GFP
130-
KHC
97-
97-
BicD
55-
α-tubulin

Fig. S5

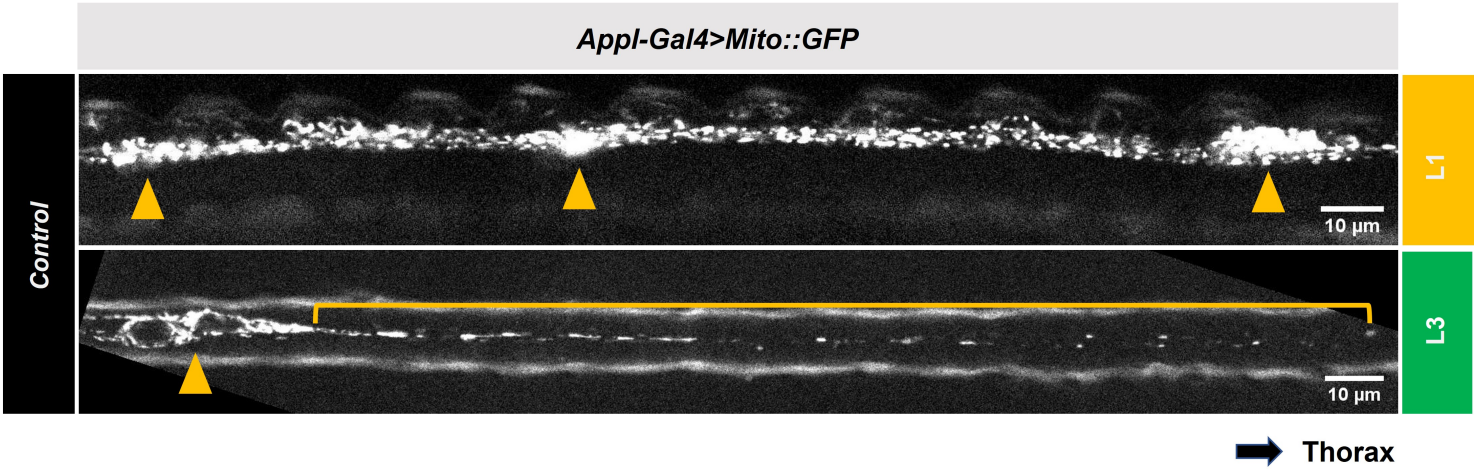

Supplementary Information

S-Tables

Table S1A: primers for cloning the sequences encoding the sgRNAs into the *Drosophila* transformation vector pCFD5

for guide 2	TTLL5 R339 top	5' TGC AGC GGC ATC CAG TCG AGG AAG
	TTLL5 R339 rev	5' AAA CCT TCC TCG ACT GGA TGC CGC
for guide 3	TTLL5 K282 top	5' TGC ATC CTA CGA AAT GAC ACG AA
	TTLL5 K282 rev	5' AAA CTT CGT GTC ATT TCG TAG GA
for guide 4	TTLL5 E517 top	5' TGC AAG ATT GAT TTC CAG TAG CCA
	TTLL5 E517 rev	5' AAA CTG GCT ACT GGA AAT CAA TCT
for guide 5	TTLL5 R376 top	5' TGC ATG GTC ACA AAT GTG ATT TGA
	TTLL5 R376 rev	5' AAA CTC AAA TCA CAT TTG TGA CCA

Table S1B: templates to introduce point mutations

TTLL5^{R339A}
= Arg (AGG) -> Ala (**GCT**) on the reverse strand; introducing an AluI site (AGCT) at the same time; PAM (underlined) on the other strand (5'TGG) 5'GAATTATAGCAAGTTGTTGGTTTAGTTACCGAATTAACAATAAATATTCC**AGC**T'CCTCGACTGGATGCCGCTGGCTTAACTATCCATGGTCCGCGATGCTTGTT
TTLL5^{E517A}
= Glu (GAA) -> Ala (**GCC**) on the reverse strand; introducing a HaeIII site (GGCC) at the same time; PAM (underlined) on this strand (5'TGG) 5'ACCTTAGTGTCCAAAGGACTATCCACACCCATTGACGGCGATAGATTGAT**GGC**CAGTAG'CCATGGCTTAAGTGCGTTGTCTATTAATATATCGAATCCATACAGCTCAA
TTLL5^{P522A}
= Pro (CCG) -> Ala (GCG) on the reverse strand; introducing a BsaHI site (GRCGYC) at the same time; PAM (underlined) on this strand (5'TGG); grey nucleotide changes that are silent mutations to prevent multiple recognition after DNA was cut 5'GTCTGCCATCAGACATGACTTAACCTTAGTGTCCAAAGGACTATCCACACCCATTGA**CGC**CGATAGATTGATTTC**G**AG**A**AG'CCATGGCTTAAGTGCGTTGTCTATTAATATATCGAATCCATACAGCTCAA

Table S2: Tissue specific expression of the 11 *Drosophila TTLL* genes

TTLL1A	testis	imaginal disc			
TTLL1B	testis	imaginal disc			
TTLL3A					
TTLL3B	testis	imaginal disc	accessory gland	central nervous system	
TTLL4A	testis	imaginal disc	ovary	central nervous system	
TTLL4B	testis	imaginal disc	accessory gland	fat body	
TTLL5	ovary	imaginal disc	testis	accessory gland	central nervous system
TTLL6A	testis	imaginal disc	accessory gland		
TTLL6B	testis	imaginal disc	accessory gland	fat body	
TTLL12	central nervous system	carcass	ovary/head/ imaginal disc	fat body	
TTLL15					

Table S3 Number of peptides of TBA1/3/4 found by MS

Isoform	***w***	***TTLL5^{pBac}***	***TTLL5^{MiEX}***
		(PSM value)	

TBA1/3	56	29	7
TBA4	12	12	4

Supplementary Information

Legends for **Fig. S1-S5 & Mov. S1-S5**

Fig. S1: Example mass spectrum for C-terminal peptides. A) Example of a mass spectrum of Glutamylation of the C-terminal domain of the TBA1/3 isoform by PEAKS and Easyprot search engines. B) Example mass spectrum of the C-terminal domain of the TBA4 isoform by the MSfragger search engine.

Fig. S2: TTLL5 was stably expressed in all Crispr/Cas9 generated *TTLL5* mutants. TR**K**D283N refers to a more complex mutation in which the codons TR**K**D283 were replaced by a N. All Crispr/Cas9 generated *TTLL5* mutations were analyzed hemizygously over *Df(3R)BSC679.* We, therefore, expect extracts from these animals to contain at most half the amount of TTLL5*. *w* ($TTLL5^{+}/TTLL5^{+}$) was the positive control and the null mutation $TTLL5^{MiEx}/Df(3R)BSC679$ was the negative control. The signal of an unspecific band (labeled with *) under short exposure was treated as a loading control. *w,* which contains 2 copies of the *TTLL5* allele expressed highest levels of TTLL5. Crispr/Cas9 generated *TTLL5* mutations with a single allele of *TTLL5* expressed less TTLL5 compared to *w,* but more compared to the null mutation $TTLL5^{MiEx}/Df(3R)BSC679$. The TTLL5 levels of the hemizygous point mutants were similar to the ones of the hemizygous wild type (refer to **Fig 1B**). The faint band seen in $TTLL5^{MiEx}/Df(3R)BSC679$ is probably a background band.

Fig. S3: Mass spectrometry analysis of the glycylation of the C-terminal end of the α-tubulin isoforms. A) The following Glu residues in the C-terminal peptides were found to be modified in *Drosophila* ovaries. E443, E445, E448, and E449 of TBA 1/3 were found modified by the addition of 1-2 glycines. B) The C-terminal peptides containing the full primary sequence were analyzed. The C-terminal tail of the TBA1/3 peptides with the Glycylation modifications found by MS are shown. Gly side chains were found added to E443, E445, E448, and E449 of TBA 1/3. C) The Glycylation frequency for the C-terminal peptides of *w* controls, $TTLL5^{pBac}$, and $TTLL5^{MiEx}$ mutants is shown. +1=frequency of peptides contained 1E modification. +2=frequency of peptides contained 2E modifications. Total Gly modification shows the sum of the 1E and 2E frequencies. The frequency was quantified based on the values of glycylated C-terminal TBA1/3 PSM (peptide spectrum match) divided by total PSM of the full primary C-terminal TBA1/3 sequence.

Fig. S4: *TTLL5* overexpression in ovaries neither alters Kinesin-1 heavy chain nor BicD levels. The KHC and BicD levels kept unchanged between *w* control and *Venus::TTLL5* overexpressing ovaries. α-tubulin was used as loading control.

Fig. S5: Still picture of Mito::GFP movie showing a selected region of L1 and L3 neurons in control wing nerves. Yellow triangle: cell bodies. Yellow bracket: axons.

Mov. S1 Ooplasmic streaming in *w* (control; 2 ooplasms)
Mov. S2 Ooplasmic streaming in *TTLL5*^{MiEx} (2 ooplasms)
Mov. S3 Ooplasmic streaming in *TTLL5*^{E517A} (2 ooplasms)
Mov. S4 Ooplasmic streaming in *Venus::TTLL5; TTLL5*^{MiEx} (2 ooplasms)
Mov. S5 Appl-Gal4>Mito::GFP trafficking in the L1 vein. Top movie: control; bottom movie: *TTLL5*^{E517A}**.**
Mov. S6 Appl-Gal4>Mito::GFP trafficking in the L3 vein. Top movie: control; bottom movie: *TTLL5*^{E517A}**.**